REPORT DOCUMENTATION PAGE

Form Approved
OMB No. 0704-0188

1. REPORT DATE *(DD-MM-YYYY)*	2. REPORT TYPE	3. DATES COVERED *(From - To)*
04/22/2004	final	07/01/2000-12/31/2003

4. TITLE AND SUBTITLE
Physical, Chemical, and Mechanical Bonding Concept/Mechanisms for Joining Steel and Composite Sections

5a. CONTRACT NUMBER

5b. GRANT NUMBER
N00014-00-1-0680:P00001

5c. PROGRAM ELEMENT NUMBER

6. AUTHOR(S)
Vijay Gupta

5d. PROJECT NUMBER

5e. TASK NUMBER

5f. WORK UNIT NUMBER

7. PERFORMING ORGANIZATION NAME(S) AND ADDRESS(ES)
Regents of the University of California, Los Angeles
Office of Contract and Grant Administration
10920 Wilshire Blvd, Suite 1200, Los Angeles, CA 90024-1406

8. PERFORMING ORGANIZATION REPORT NUMBER
24889

9. SPONSORING/MONITORING AGENCY NAME(S) AND ADDRESS(ES)
Regents of the University of California, Los Angeles
Office of Contract and Grant Administration
10920 Wilshire Blvd, Suite 1200, Los Angeles, CA 90024-1406

10. SPONSOR/MONITOR'S ACRONYM(S)

11. SPONSOR/MONITOR'S REPORT NUMBER(S)

12. DISTRIBUTION/AVAILABILITY STATEMENT
UU/approved for public release; distribution unlimited.

13. SUPPLEMENTARY NOTES

14. ABSTRACT
Silane-based chemistries on stainless steel substrates have been investigated to develop reliable stainless steel/E-glass composite sections. A chemistry has been uncovered that leads to a joint stronger than one of the substrate (composite). Effects of moisture and seawater on the fracture energies of the joints were also determined. Silane layers have been found that control the fracture path through the multilayer joint assembly in a way that improves the long-term fracture reliability by a factor of 5 over regular non-silane joint chemistries. The degrading effect of seawater was dramatic and the use of silane was not as effective as that against moisture attack. The intrinsic fracture energy of the joint was also measured by carrying out experiments at cryogenic temperatures, which can be used as a local failure criterion in design simulations of large structures. The intrinsic-to-total toughness relationship was experimentally obtained for the steel/composite joint, which provides the necessary scaling law for designing joints in large-scale structures based on the lab data. The dynamic tensile strengths of various interfaces in the joint were also measured.

15. SUBJECT TERMS
Fracture Energy, Joints, Moisture, Joint Reliability, Double Cantilever Experiment, Dynamic Strength, Joint Strength, Steel/Composite Joint.

16. SECURITY CLASSIFICATION OF:			17. LIMITATION OF ABSTRACT	18. NUMBER OF PAGES	19a. NAME OF RESPONSIBLE PERSON
a. REPORT	b. ABSTRACT	c. THIS PAGE			Vijay Gupta
unclassified	unclassified	unclassified	UU		19b. TELEPHONE NUMBER *(Include area code)* (310) 825-0223

Physical, Chemical, and Mechanical Bonding Concept/Mechanisms for Joining Steel and Composite Sections

Final Report

Submitted by

Vijay Gupta
vgupta@ucla.edu
Telephone: 310-206-2302

Professor of Mechanical and Aerospace Engineering
Professor of Materials Science and Engineering

Abstract

Silane-based chemistries on stainless steel substrates have been investigated to develop reliable stainless steel/E-glass composite sections. A chemistry has been uncovered that leads to a joint stronger than one of the substrate (composite). Effects of moisture and seawater on the fracture energies of the joints were also determined. Silane layers have been found that control the fracture path through the multilayer joint assembly in a way that improves the long-term fracture reliability by a factor of 5 over regular non-silane joint chemistries. The degrading effect of seawater was dramatic and the use of silane was not as effective as that against moisture attack. The intrinsic fracture energy of the joint was also measured by carrying out experiments at cryogenic temperatures, which can be used as a local failure criterion in design simulations of large structures. The intrinsic-to-total toughness relationship was experimentally obtained for the steel/composite joint, which provides the necessary scaling law for designing joints in large-scale structures based on the lab data. The dynamic tensile strengths of various interfaces in the joint were also measured.

KEYWORDS: Fracture Energy, Joints, Moisture, Joint Reliability, Double Cantilever Experiment, Dynamic Strength, Joint Strength, Steel/Composite Joint.

1. Motivation for Research

R&D efforts are presently underway at ONR and NSWCCD for making future lightweight highly mobile ship structures using mixed steel and composite construction. The plan is to make the bow and stern of the ship using fiber glass-reinforced vinyl ester resin, while retaining steel for the ship's mid-section. Because of the rather large mismatch between the elastic stiffness of the two materials, a major challenge in realizing such a composite ship structure is to design and construct reliable composite and steel section joints that can withstand the static, dynamic, and fatigue loads, during operation.

The focus of this research was to explore chemical bonding concepts/mechanisms to join composite and steel sections and characterize them under static and dynamic loads in the presence of moisture and seawater environment.

2. Technical Objectives

(1) Fabricate stainless steel/E-glass vinyl ester composite joints using novel chemical and mechanical routes, (2) characterize the fundamental interface mechanical properties of intrinsic tensile strength, intrinsic toughness, and total toughness using novel experiments, and (3) experimentally determine the relationship among the latter to answer issues of size effects in joint design and to promote further development of plasticity theories for layered systems. The fundamental parameters that characterize the fracture behavior of the joints are the total joint toughness or the fracture energy G_c, the intrinsic toughness G_o, and the intrinsic strength σ_0. Their definitions and relationship among them is depicted in Fig. 1.

3. Technical Approach

The specific materials studied in this program are summarized in Fig. 2. Silane-based chemistries were used to bond the steel and composite sections. The specific reactions that allow attachment of silane onto the steel surfaces are summarized in Figs. 3 (a) & (b). The goal was to optimize adhesion between the composite and steel sections. Besides, interfaces were weakened so as to generate total toughness data for different levels of intrinsic toughness levels. This resulted in developing the nonlinear relationship between the intrinsic and total toughness for the composite/steel joints as needed to develop the scaling laws for transferring the lab data to large structural joints.

The total toughness was measured using a double cantilever beam experiment (Fig. 4). This setup was also equipped with an environmental cell so that toughness experiments could be carried out at cryogenic temperatures (Fig. 5). The idea was to progressively reduce the plastic component of the deformation during interface separation, with the hope that the measured toughness values will approach those of the intrinsic toughness at the lowest temperature.

The intrinsic strength was measured using a laser-induced stress wave experiment. In this experiment, a 16 to 20 nanoseconds long pressure pulse was generated in the composite beam towards the steel plate that is bonded on its top face (Fig. 6). The pressure pulse reflects into a tensile wave from the free surface of the steel and loads the composite/steel interface in tension. The interface separates if the tensile stress exceeds the joint strength. An interferometer is used to record the free surface velocities and this information is used to calculate the local interfacial tensile stress.

The above experiment was also adapted to measure the intrinsic toughness of the joint wherein a well-characterized interfacial flaw was implanted at the steel/composite interface and loaded by the laser-generated stress wave (Fig. 7). Crack initiation occurred at a critical stress wave amplitude which in turn was interferometrically recorded. The measured stress wave profile was then used in conjunction with the known interface crack geometry to compute the energy release rate using a dynamic fracture mechanics-based simulation. The computed value equals the joint's intrinsic toughness at crack initiation since interface decohesion is accomplished at strain rates of 10^8 s^{-1} and higher.

The above apparatuses were used to determine both the intrinsic and total toughnesses for the steel/composite joints modified by various silane surface treatments.

4. Results

For the purpose of brevity, the details of results will be provided in the forthcoming articles here we summarize the key results and contributions, which are directly useful to NSWCCW and other collaborators in the program.

1. Appropriate silane (trimethoxyvinylbenzylamine) chemistry for the treatment of superaustenetic stainless steel surfaces have been determined. When bonded to E-glass composite using Hysol EA 9394 epoxy (also determined as part of this research) a rather strong composite-to-steel bond resulted. Double cantilever beam tests confirmed that this bond was tougher than the inherent epoxy and composite structures, as the total joint toughness was measured to be higher than that of the epoxy and the interlaminar composite toughness. Figure 8 shows the stable load vs. load point curves for the DCB experiment and the resulting G_c values calculated from them. As shown in Figs. 9 (a-d), this enhanced toughness is a direct result of simultaneous formation of two cracks during joint fracture. The first crack is at the epoxy/composite interface while the second crack takes the form of interlaminar delamination at the first ply interface nearest the joint. Figure9 (e) shows the micro x-ray analyses results from bare epoxy and composite surfaces that were used to determine the locus of failure in Figs. 9 (a-d). Figure 10 shows the schematic of the dual crack formation process with respect to the microstructure.

2. The effect of seawater and moisture on the toughness of optimized steel/composite sections was studied next.

Mechanical test results showed that the moisture affected the composite to steel interface directly, as the failure locus changed from composite delamination and cohesive failure within the epoxy to pure steel/composite interfacial failures as the duration of moisture exposure was increased (Figs. 11-12). Quantitatively (Fig. 11), the effect was dramatic as the joint toughness was found to reduce from 938 J/m^2 under ambient conditions to 573 J/m^2 after 1 day of exposure at 50 °C at 90% RH to a mere 98 J/m^2 on day 5 under similar conditions. Figure 12 shows details of micro x-ray analyses that confirmed the locus of failure after different moisture exposure times.

Interfacial designs using silane layers to address the long-term stability of steel/E-glass joints were studied. Figure 13 shows the beneficial effects of using two different silane layers (A & B) along with the chemical recipes for both silanes. The silane layer acted as a moisture barrier and led to interface-to-interface crack jumping to improve the long-term joint reliability of the joint. This is effectively shown in Figs. 14-17 for silane A by combining microscopy and micro x-ray analyses. Silane B optimizes the joint as joint failure occurred from failure within the composite (Fig. 18).

Next the effect of seawater was determined on the long-term reliability of joints. There was a dramatic reduction in the toughness of E-glass/epoxy/steel joint (Fig. 19), which could be marginally stabilized by use of silane layer on the steel beams. The relative ineffectiveness of the silane layer in stabilizing the joint against seawater attack compared to moisture is because the E-glass composite itself deteriorates with seawater. Thus, the crack propagates through the composite section avoiding the joint. The details of failure locus as determined by combining microscopy and micro x-ray analyses results are summarized in Figs 20-24. Future efforts should be focused on determining material recipes for the E-glass composite section of the joint that would protect it from seawater deterioration.

Figure 25 summarizes all the experimental data on G_c measured in this program on the steel/composite joints, including the effects of silanes, moisture and seawater.

Next the Intrinsic toughness was measured using DCB tests at cryogenic temperatures (Fig. 26) for the purposes of determining a value that could be used as a local failure criterion in large-scale simulation of joints. The results were surprising in that higher than expected values were measured.

Figure 26 also shows hitherto unattained relationship between the intrinsic to the total toughness for the steel/composite joints. It is noteworthy that such a relationship has never been obtained for any interface system in the literature. Figures 27-29 show that for both types of samples, with and without silane layers, the failure was through the formation of double cracks.

In order to further lower the interfacial energies, the moisture-segregated samples were tested at cryogenic temperatures. Rather interestingly the measured toughness values were higher than those obtained for the same samples but tested under ambient conditions (Figure 30). Thus, it appears that the low temperature lowers the kinetics of

moisture and thus stabilizes its degrading effect. The failure in all samples tested at cryogenic temperature was cohesive through the epoxy layer.

The intrinsic (dynamic) tensile strength values for epoxy/steel, epoxy/composite, epoxy/silane(A)/steel, epoxy/silane(B)/steel were determined using the laser spallation experiment. The results are summarized in Fig. 31. Interestingly, different interfaces in the joint assembly could be separated by using different laser fluences. The critical laser fluence and the associated failure loci are summarized in Fig. 32.

In order to further understand the high intrinsic toughness values, dynamic fracture toughness experiments were performed on the joints using pre-existing cracks using laser-generated stress waves, in the presence and absence of moisture. The quantification of the critical energy release rates was not done in this program but instead the feasibility of the dynamic test apparatus was demonstrated. Figure 33 clearly shows that the laser generated stress pulses can drive a pre-existing crack and that the moisture has a significant effect in controlling both the failure loci in the joint and the critical laser fluence to initiate the crack. Future work will quantify these results to obtain the dynamic fracture energy values, which are expected to be close to the intrinsic toughness values.

Intrinsic Strength and Toughness vs. Total Toughness

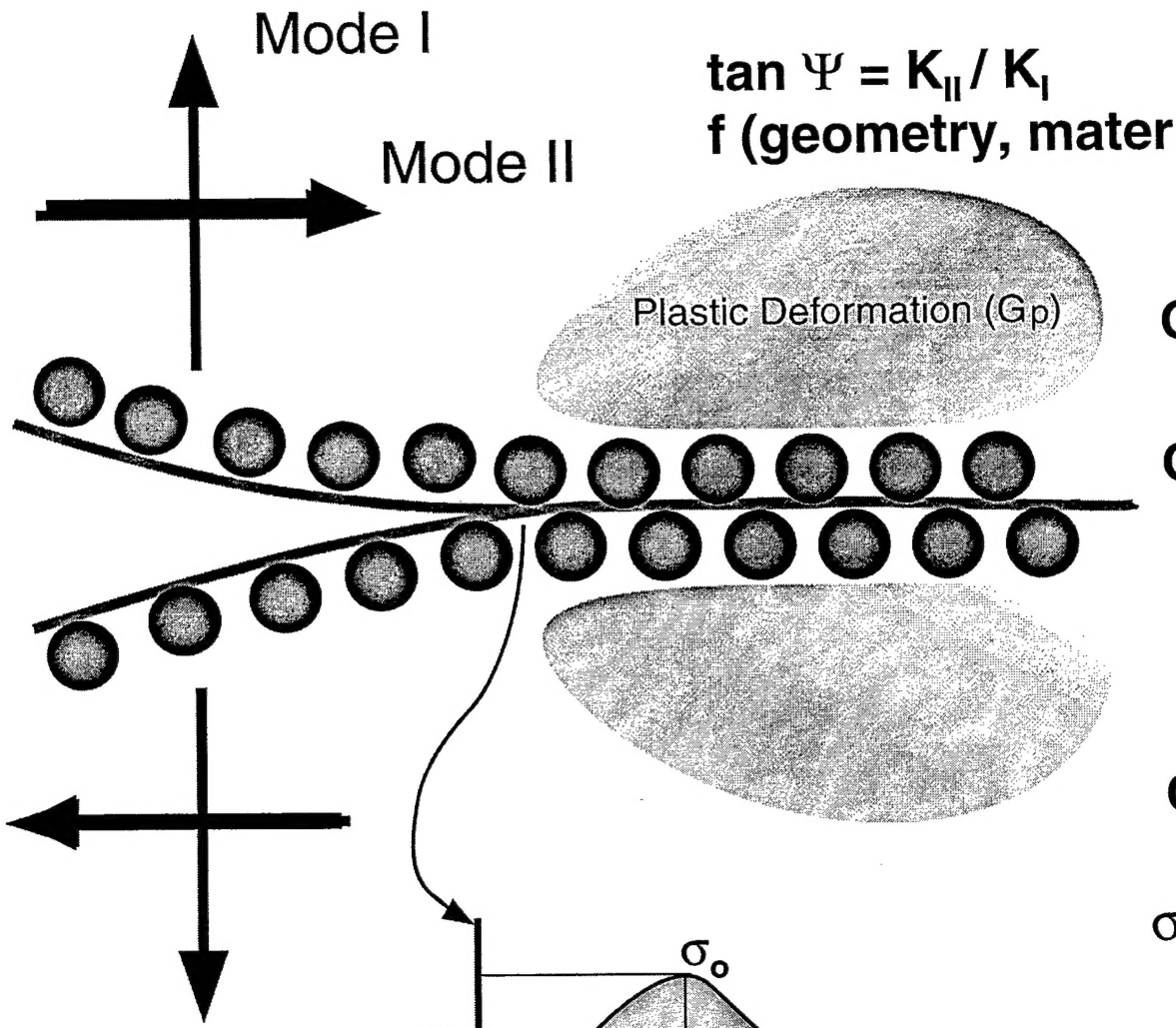

$\tan \Psi = K_{II} / K_I$

f (geometry, material, crack length)

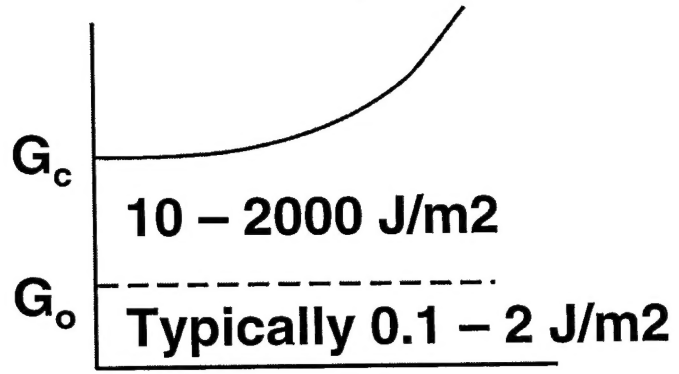

$\Psi = \tan^{-1} (K_{II} / K_I)$

$G_c = G_o + G_p$

$\sigma^2_o = c\, G_o\, E/h$

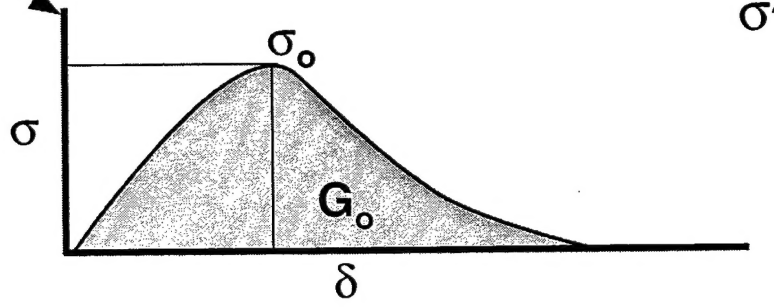

Fig. 1

Material System

- **Steel** — **AL-6XN**
- **Composite** — **E-glass Composite**

  Cytecfiberite

  Elemental Composition: Ca, Si, Cl, C, O, H
- **Epoxy** — **Hysol EA 9394**

  Part: A

  Aluminum Powder

  Bisphenol A/

  Epichlorohydrin: H, O, C1

  Silica: Si

  Part: B

  Aliphatic Amines: H, O, N

  Silica: Si
- **Silane** — **Dow Corning Z-6030**

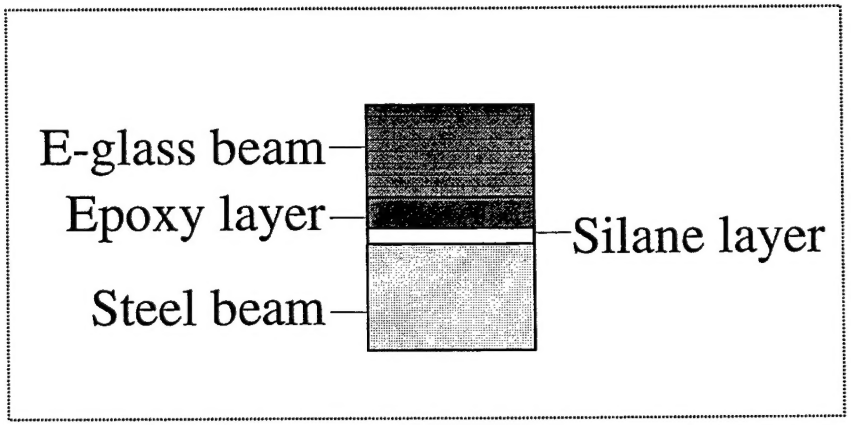

Fig. 2

Mechanism of Bonding

Organosilane:

$R_nSiX_{(4-n)}$

-R: nonhydrozylable organic radical

-X: involved with reaction with inorganic substrate

-Specific organosilane for the stainless steel

***Dow Corning* Z-6030 silane** and its chemical formula is

$$(CH_3O)_3SiCH_2CH_2CH_2OC(=O)C(CH_3)=CH_2$$

where

R → $CH_2CH_2CH_2OC(=O)C(CH_3)=CH_2$ (γ-Methacryloxypropyl)

X → $(OCH_3)_3$ (Trimethoxy)

Hydrolysis:

$$RSi(OCH_3)_3 + 3H_2O \longrightarrow RSi(OH)_3 + 3CH_3OH$$

$RSi(OH)_3$ (Silanol)

$$\oplus \downarrow 2RSi(OH)_3$$

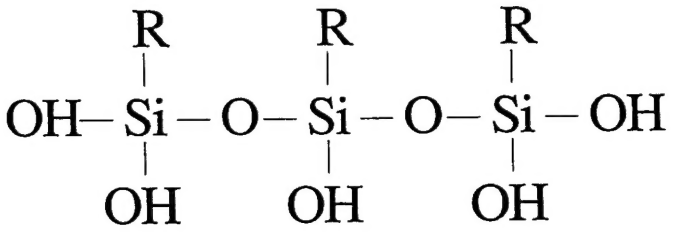

-1% Organosilane $RSi(OCH_3)_3$ with 95/5 mixture CH_3OH+H_2O

-PH 4.5 adjusted with acetic acid

Fig. 3a

Mechanism of Bonding

Condensation

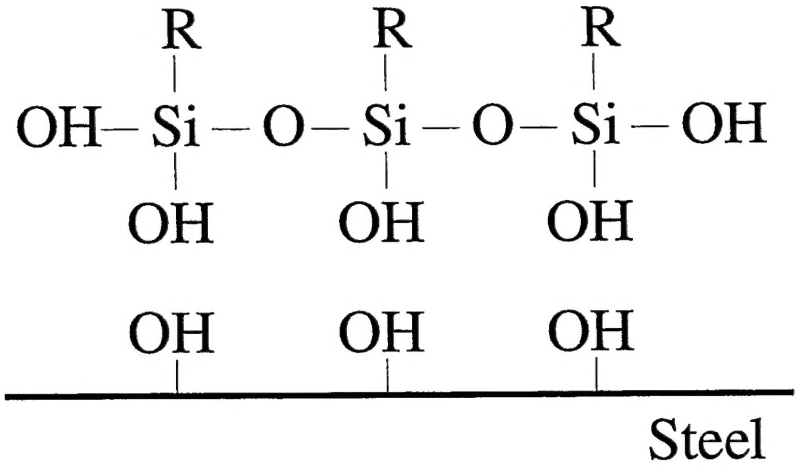

-Degrease: dip steel in DI water for surface hydration

Hydrogen Bonding

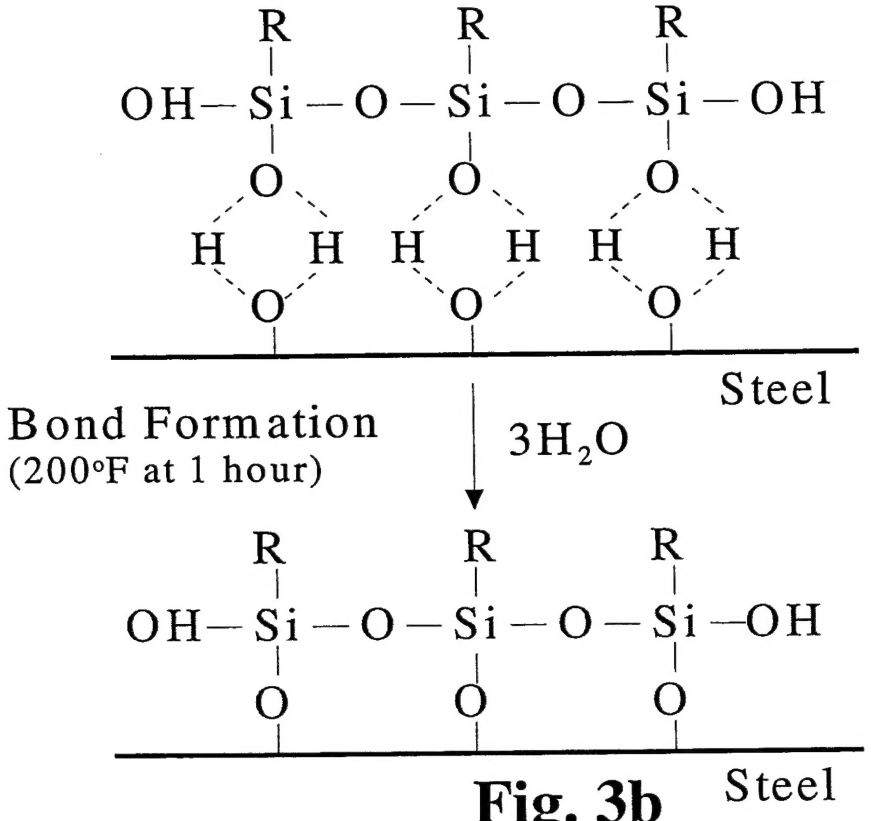

Fig. 3b

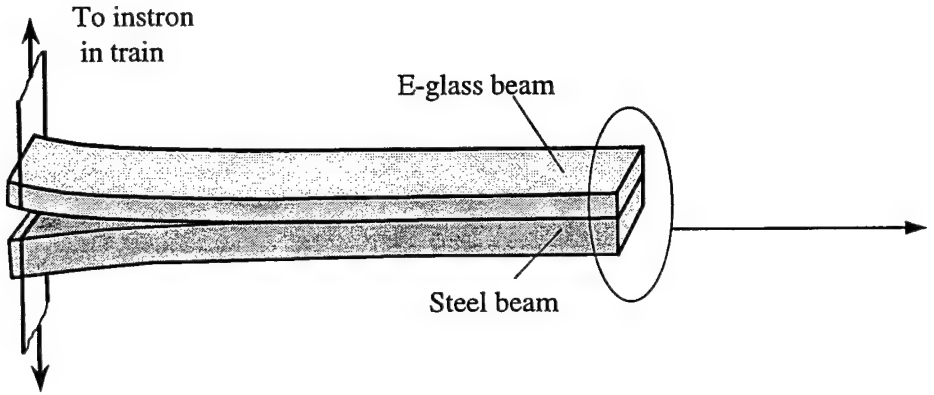
To instron
in train
E-glass beam
Steel beam

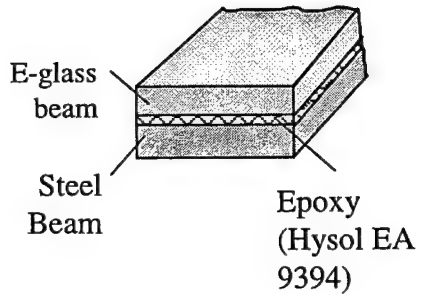
E-glass
beam
Steel
Beam
Epoxy
(Hysol EA
9394)

Fig. 4

Double Cantilever Beam Experiments at Ambient and Cryogenic Temperatures

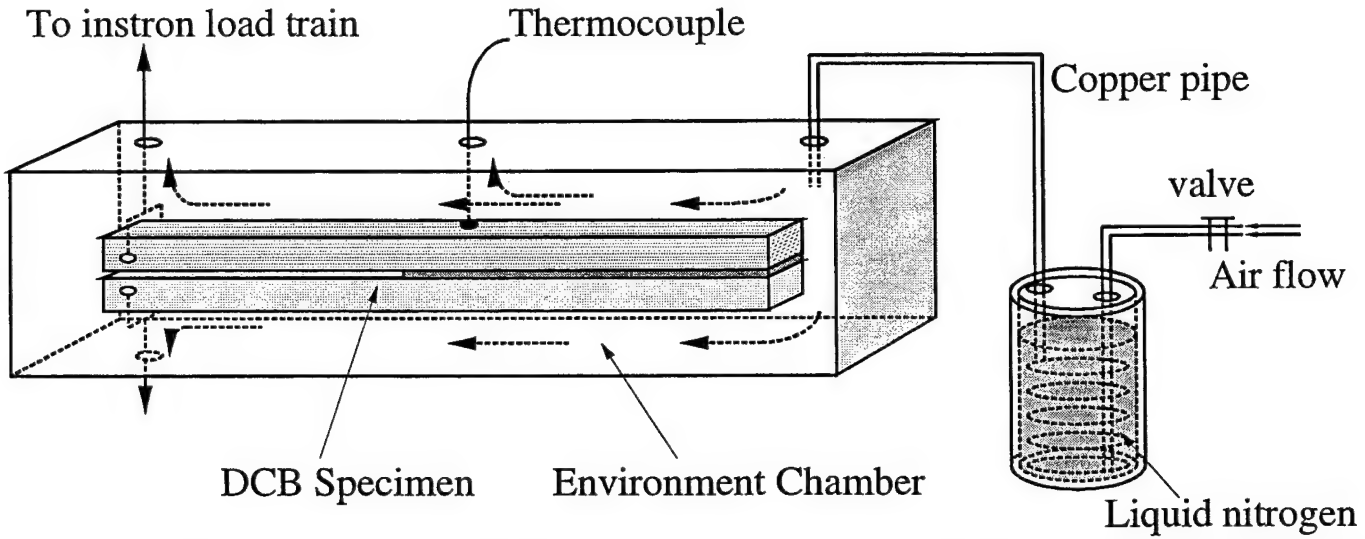

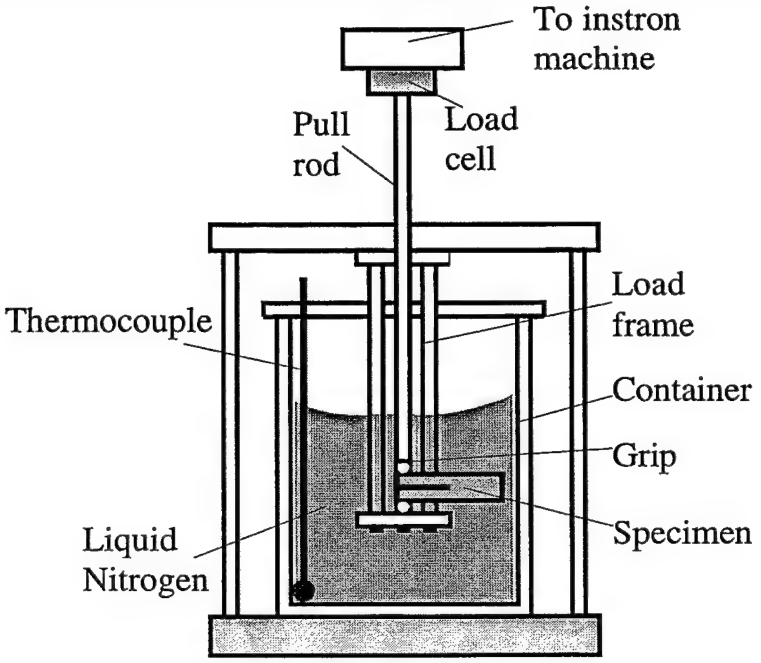

Fig. 5

Dynamic Measurement of σ_0 of Steel/E-glass joints by using Laser-generated Stress Pulses

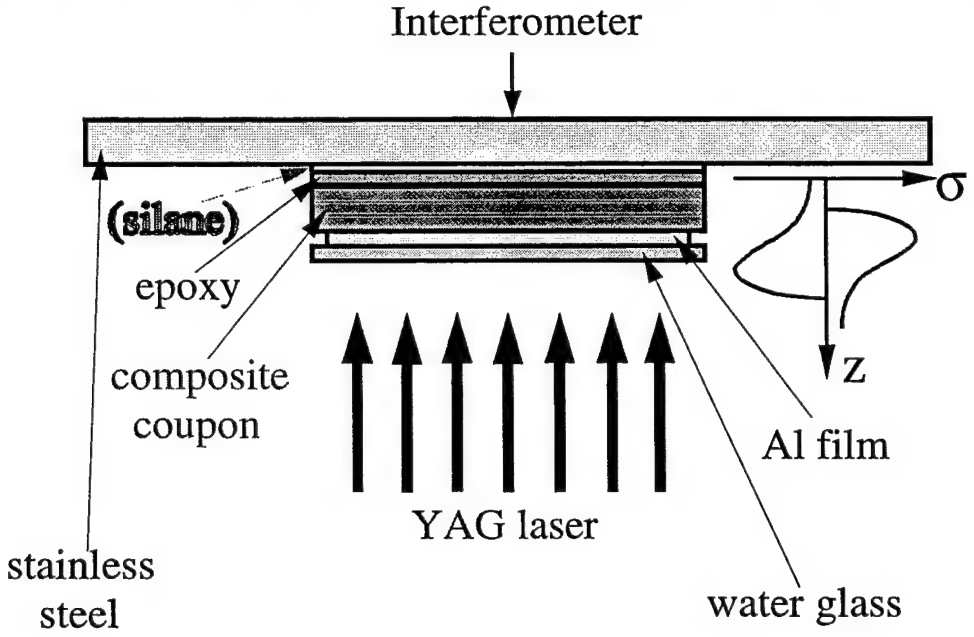

Fig. 6

Dynamic Measurement of G_0 of Steel/E-glass joints by using Laser-generated Stress Pulses

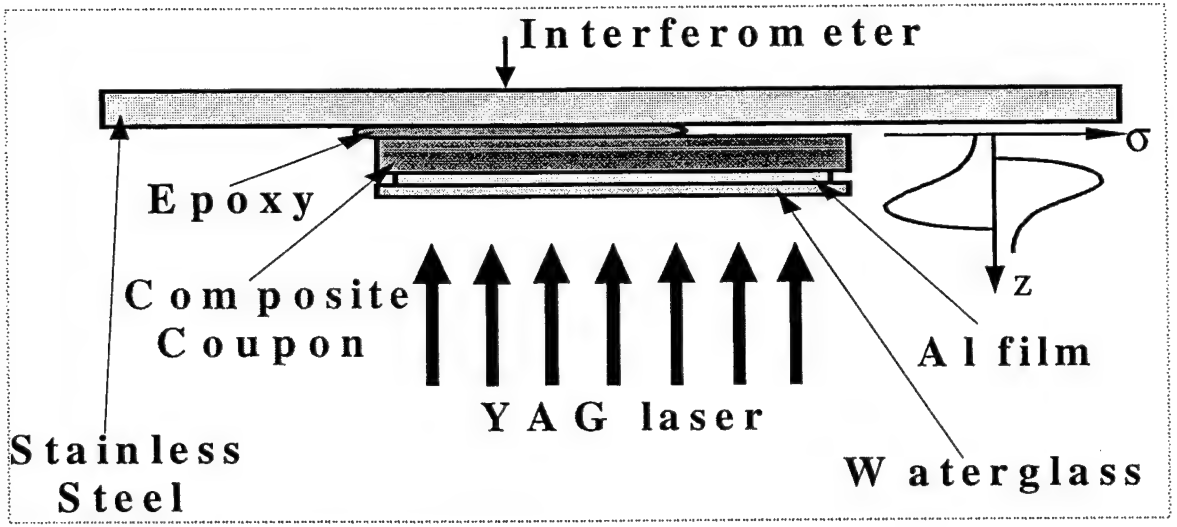

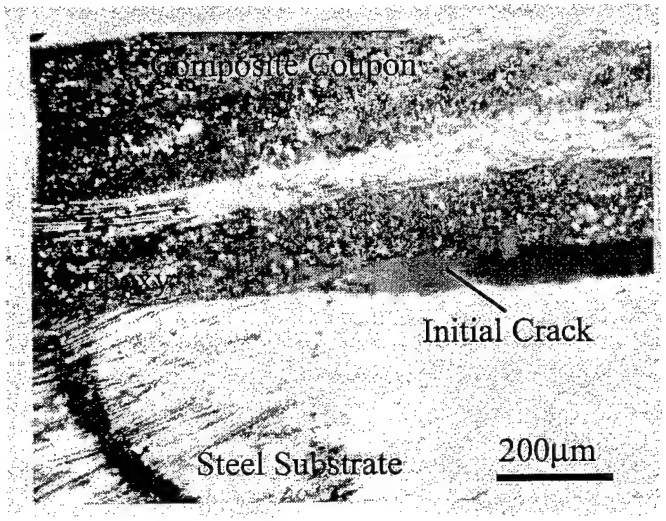

Fig. 7

A focused view at the crack tip, with an initial crack length of 1mm

Table 1. Thickness of various layers

Layer	Thickness (μm)
Composite	700 ±10
Steel	724
Epoxy	71±15
Al film	0.5
Waterglass	5

Table 2. The dimension of composite coupon

Width (mm)	4.7
Length (mm)	3.0

Experimental Data

(at room temperature without humidity treatment)

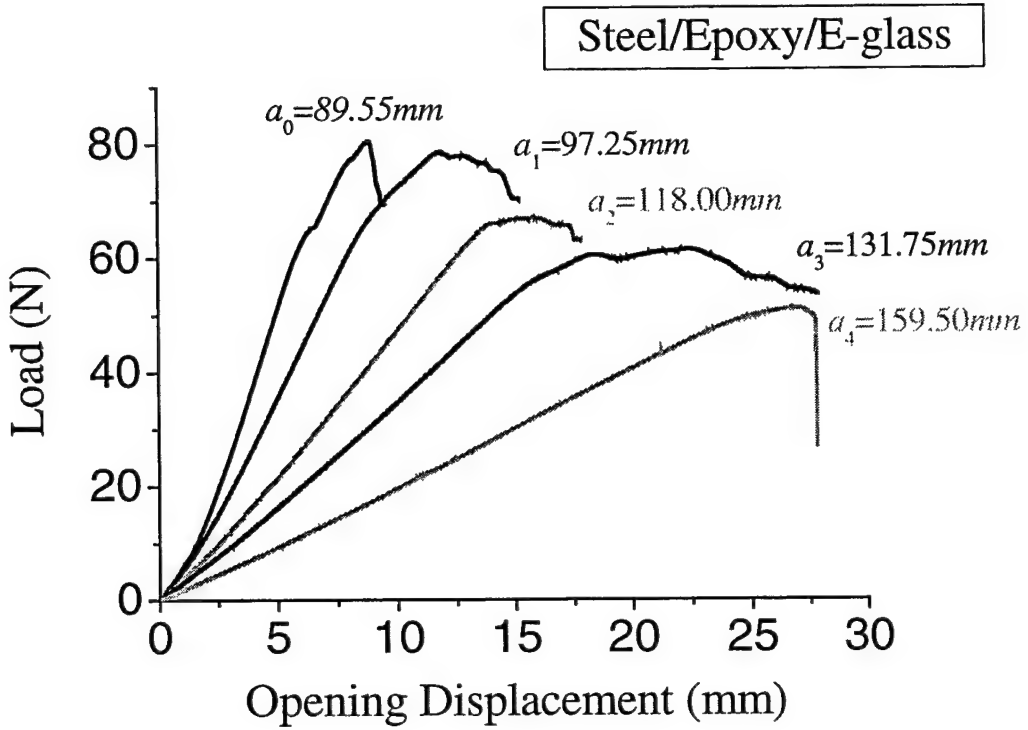

Experimental Data G_c (J/m^2)	1	957
	2	837
	3	880
	4	1037
Average of G_c (J/m^2)		928

Fig. 8

Figure 4-5: Region 4 – Steel, Hysol EA9394

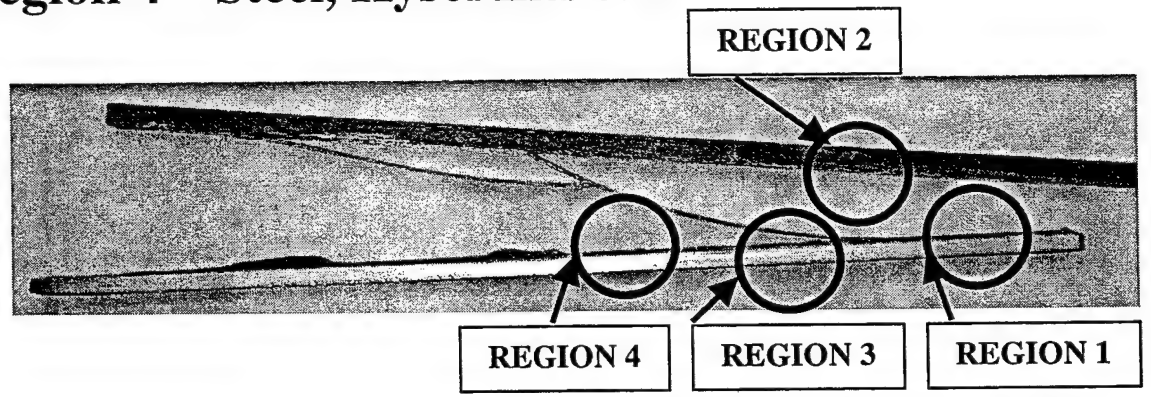

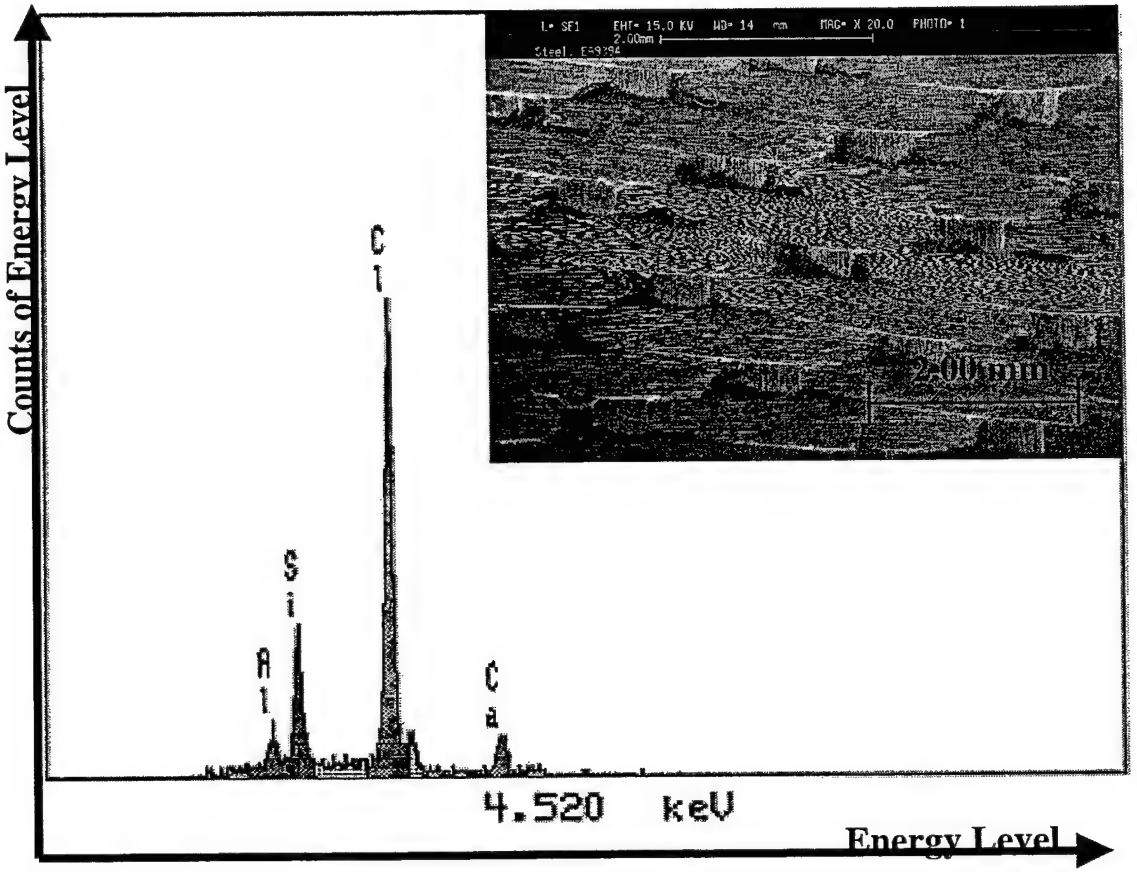

Fig. 9a

Figure 4-3: Region 2 – Composite

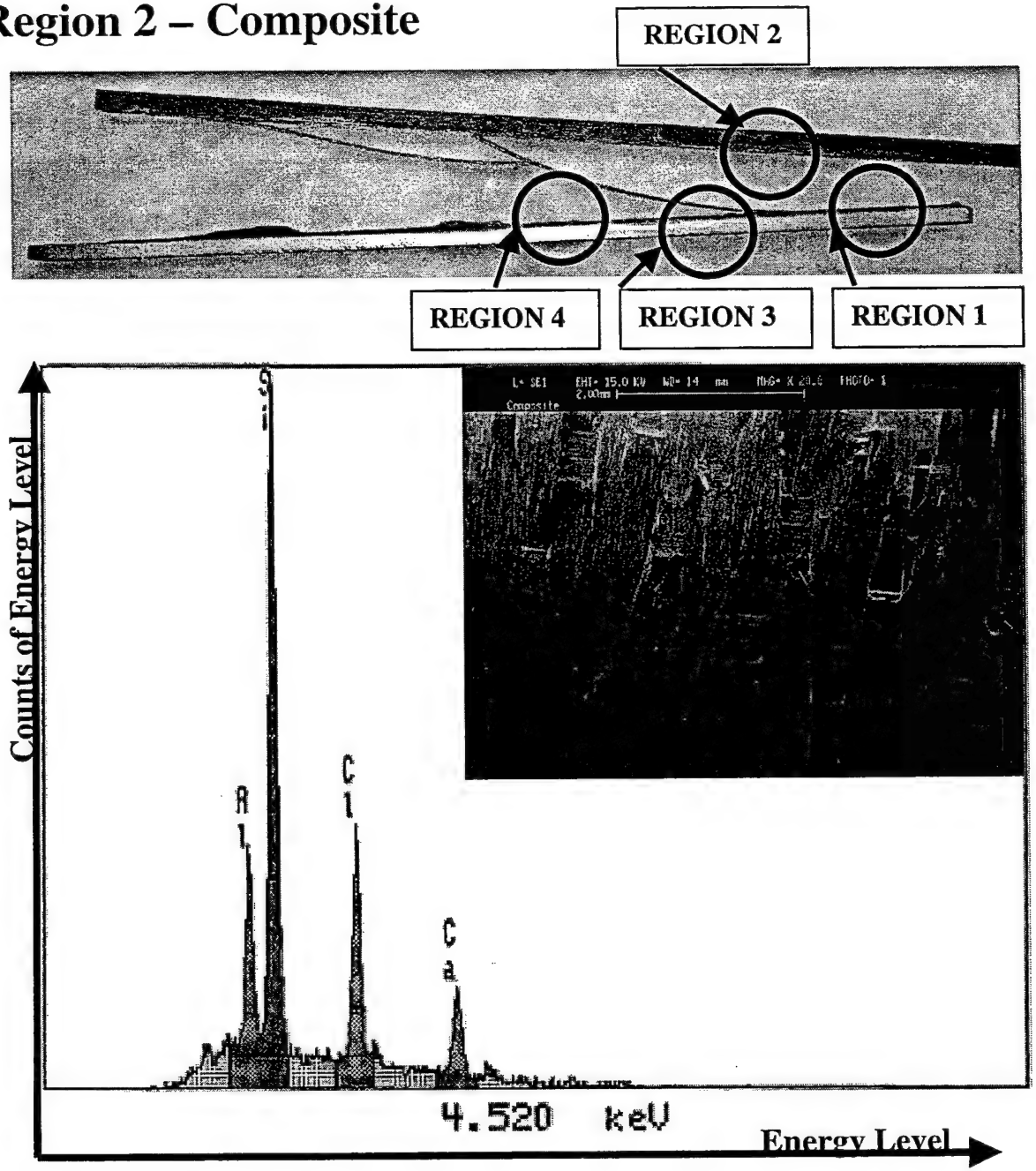

Fig. 9b

Figure 4-4: Region 3 – Steel Mid End

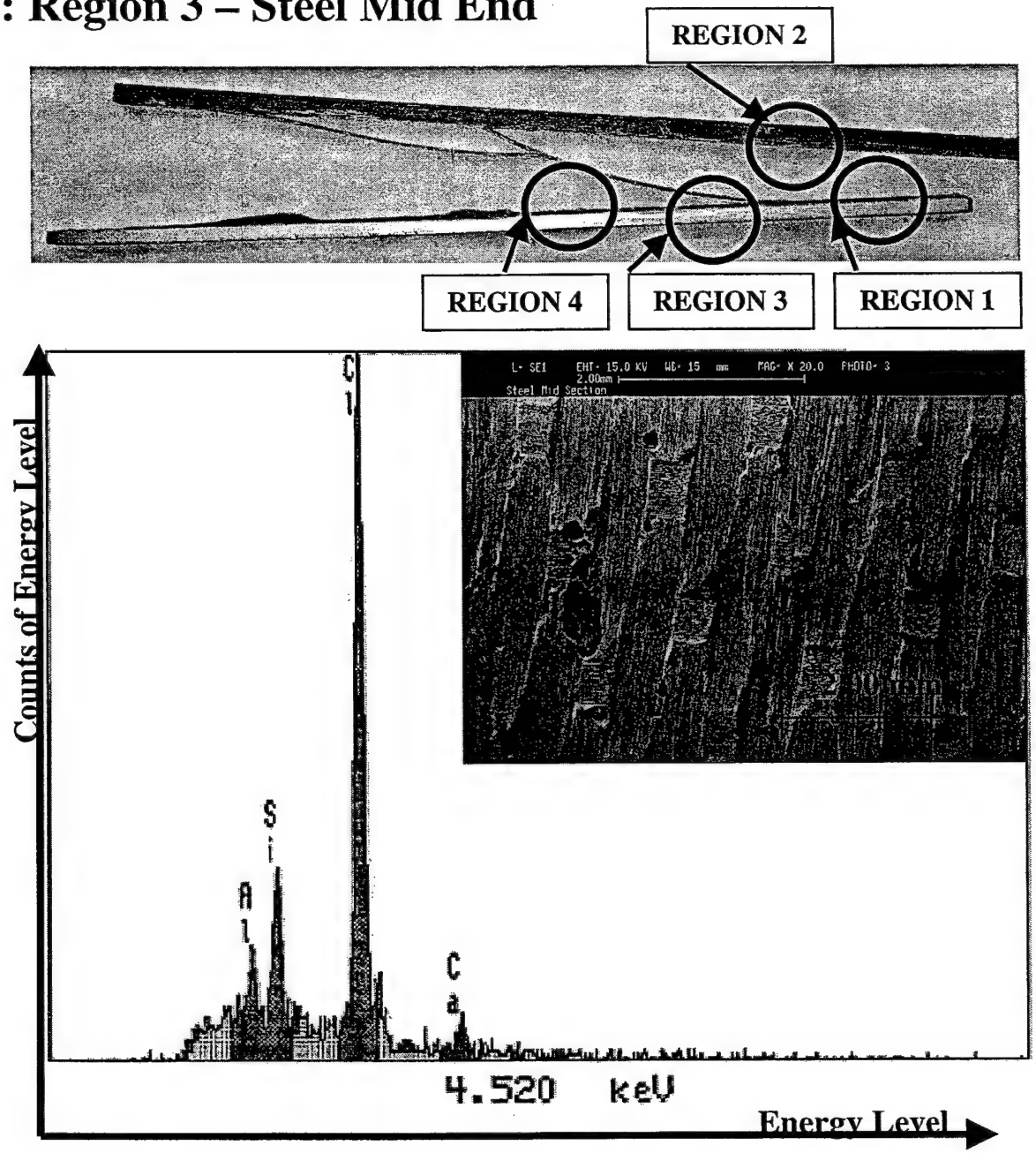

Fig. 9c

Figure 4-2: Region 1 – Steel Composite End

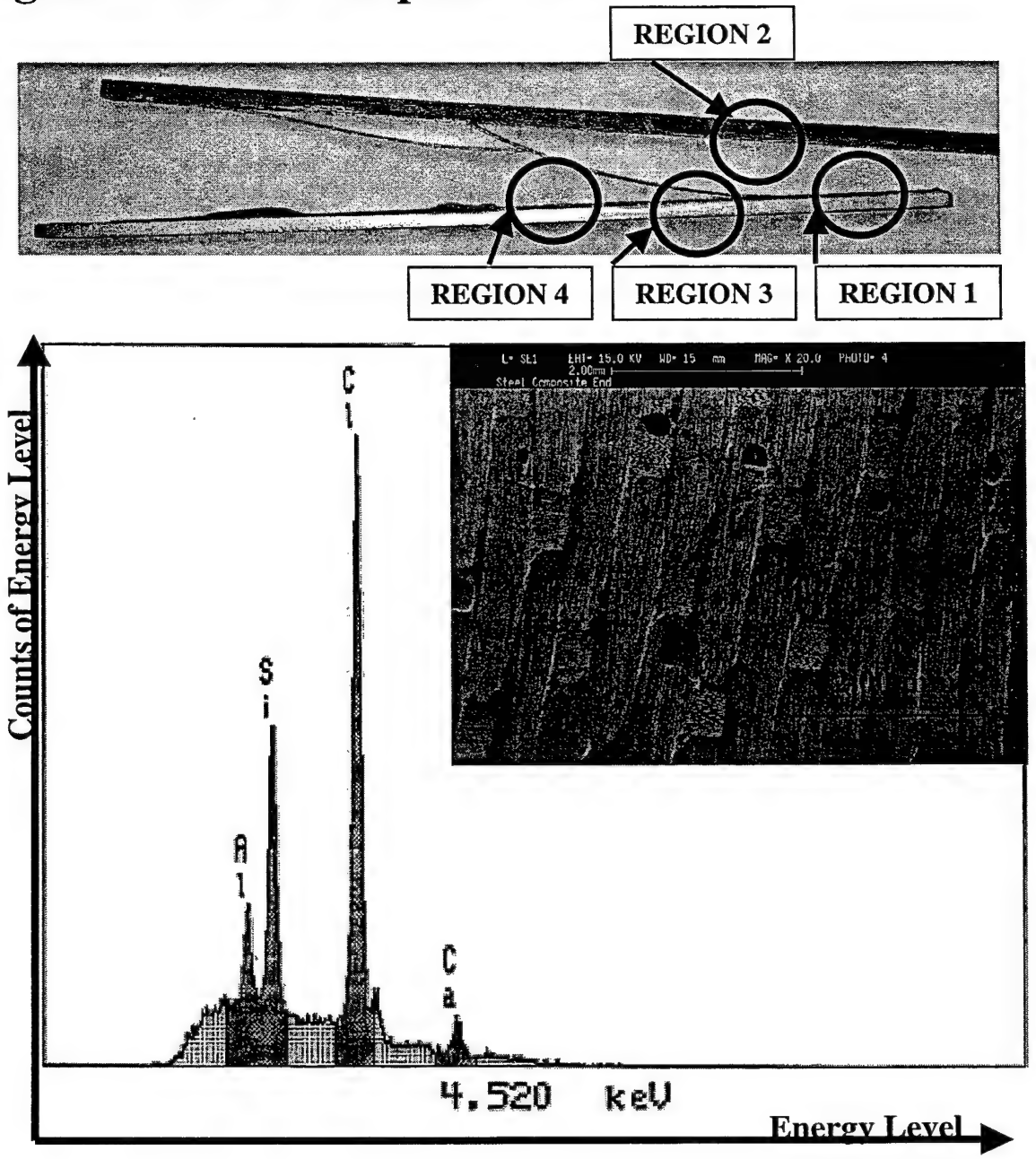

Fig. 9d

EDX Analysis on Pure E-glass

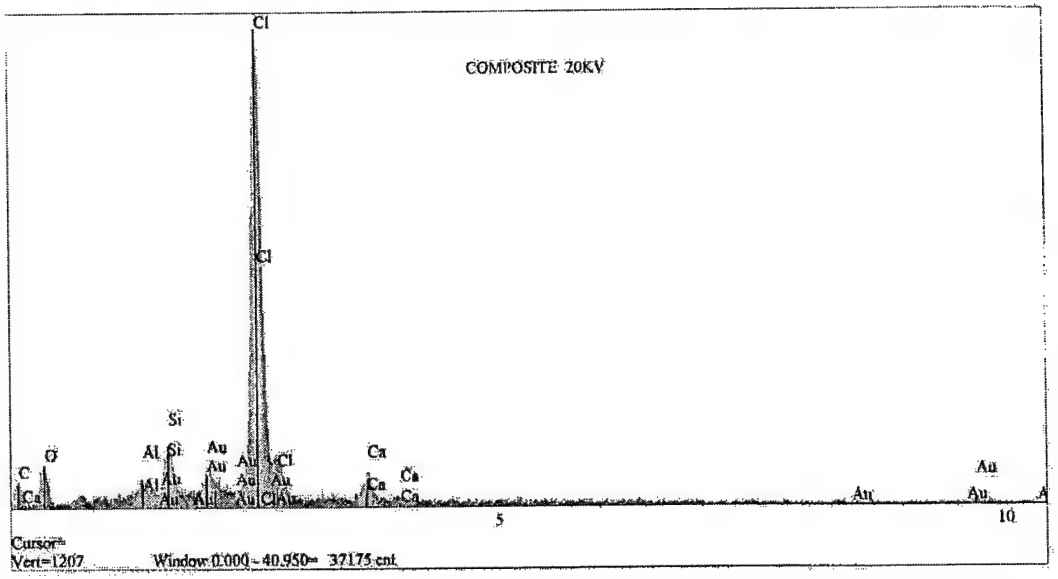

EDX on Silane Layer Coated on Steel Surface

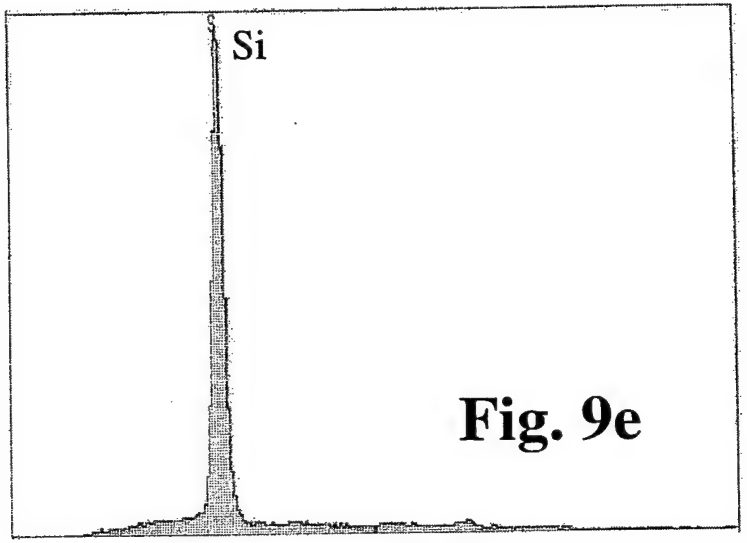

Fig. 9e

Delamination Mechanism of Composite

Thickness of epoxy: 105±15μm

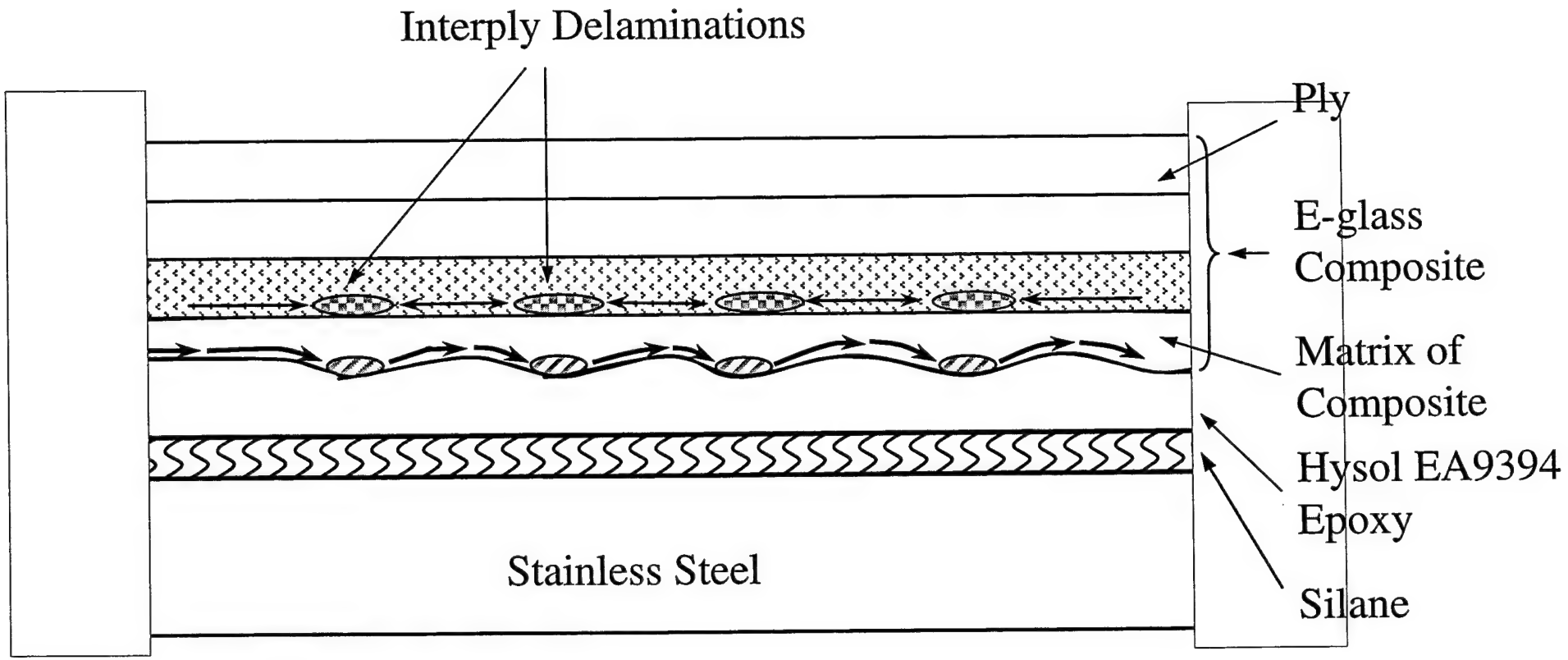

Fig. 10

Effect of Humidity on Fracture Energies of Joints Steel/Epoxy/E-glass

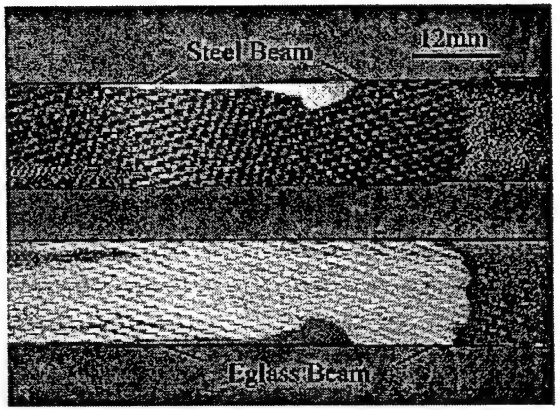

a- 1 day

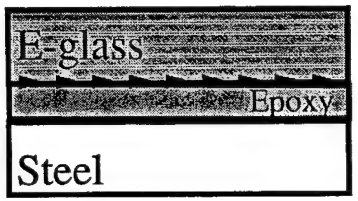

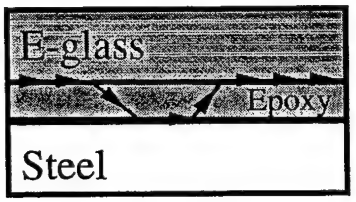

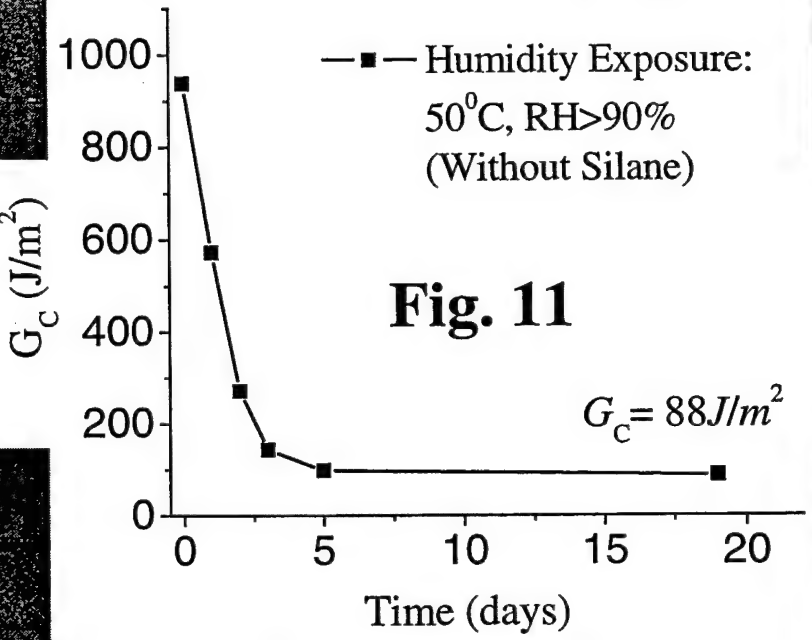

Fig. 11

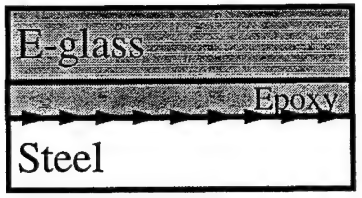

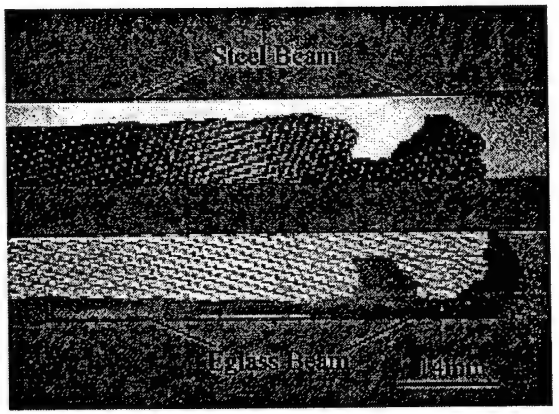

b- 2 days

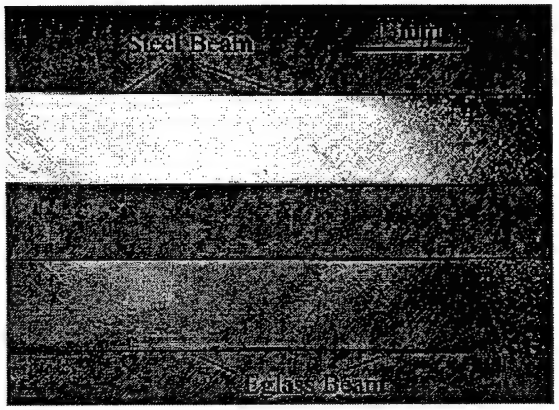

c- 3 days

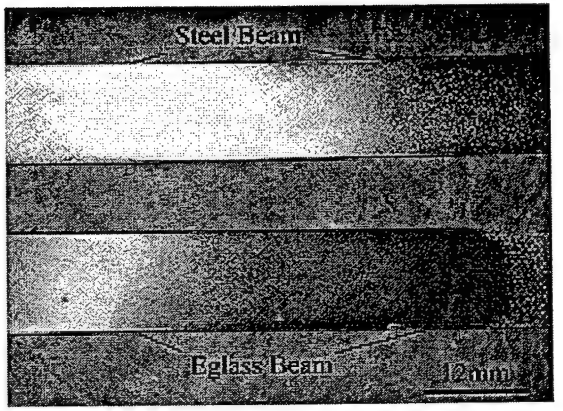

d- 5 days

Steel/Epoxy/E-glass (After 19 days Humidity Exposure)

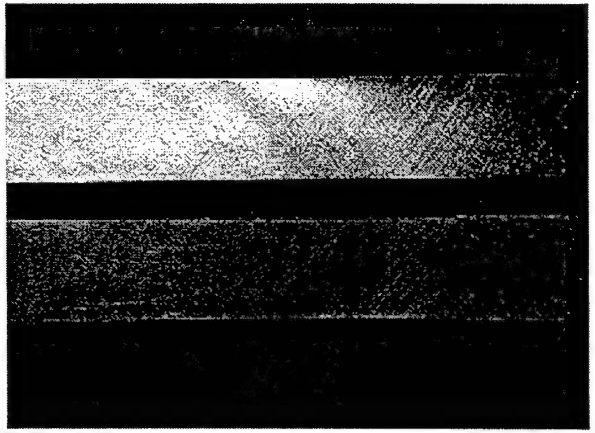

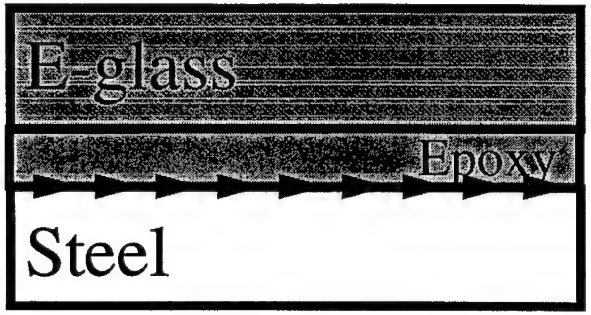

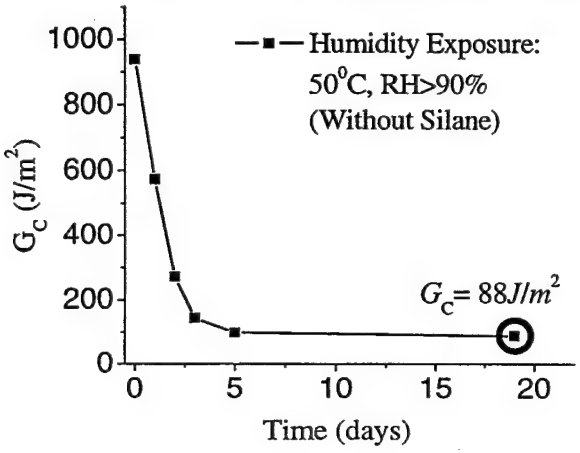

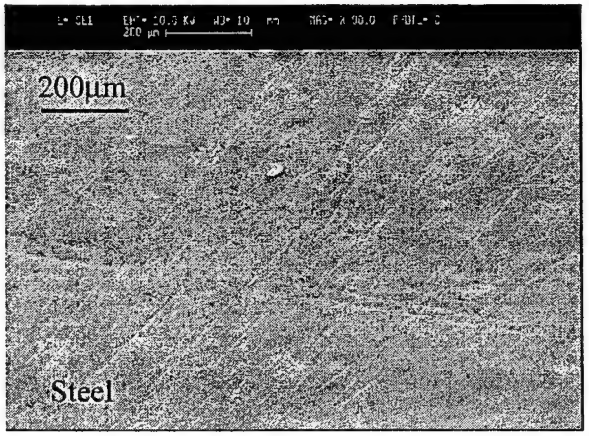

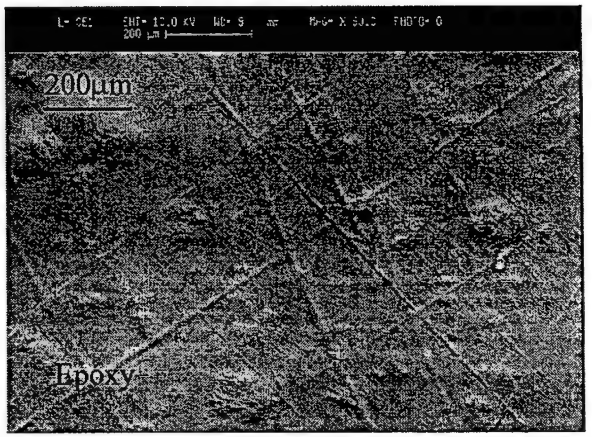

SEM crack surfaces

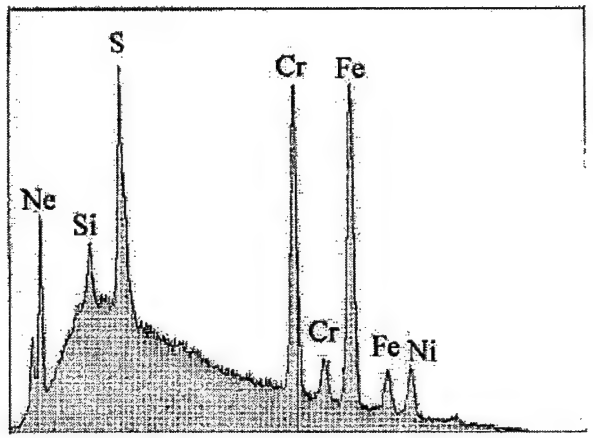

EDX analysis on steel part

Fig. 12

Note: There is no signal on the epoxy part in EDX analysis

Effect of Silane Chemistry on Fracture Energies of Joints

- **Recipe A**

90% methanol +10% DI water

↓

adjust pH 4-5 by using acetic acid

+

1% Silane

↓

apply on the clean and degreased steel surface

↓

Curing @ 200-220°F

- **Recipe B**

100% methanol

↓

adjust pH 3.5-4.5 by using acetic acid

+

3% Silane

↓

apply on the clean and degreased steel surface

↓

Curing @ 200-220°F

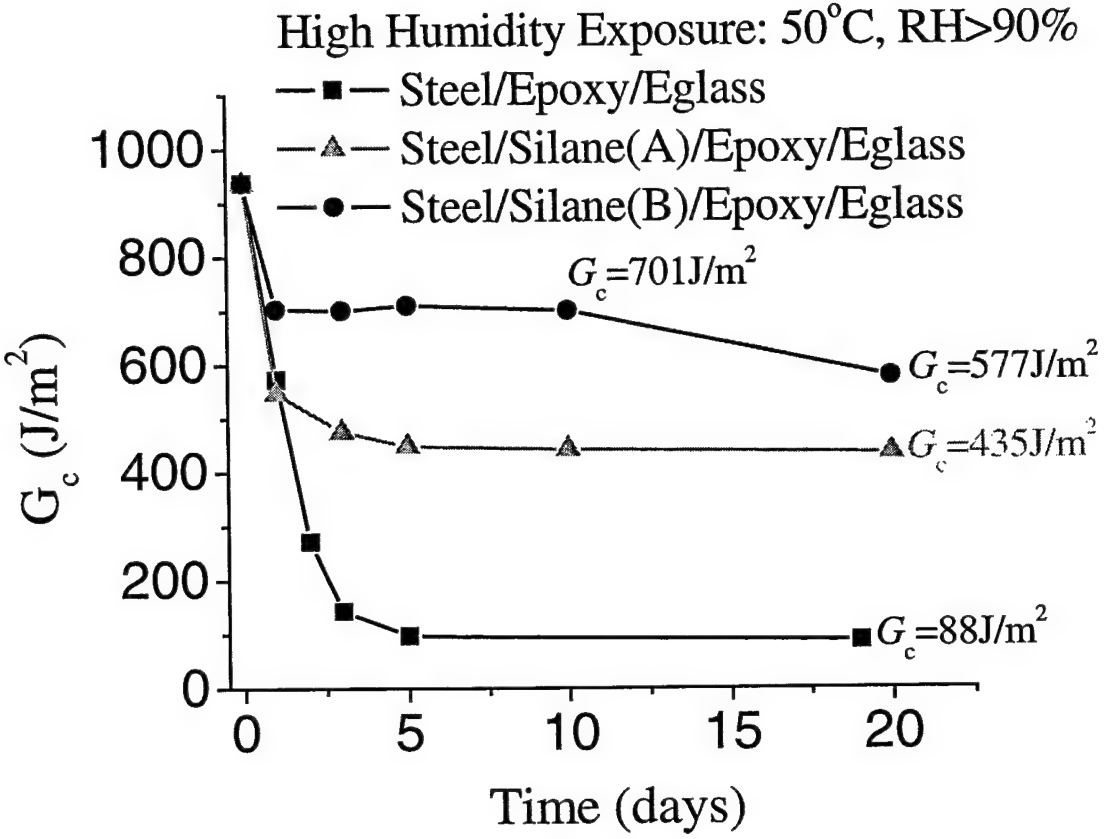

Fig. 13

Effect of Humidity on Fracture Energies of Joints Steel/Silane(A)/Epoxy/E-glass

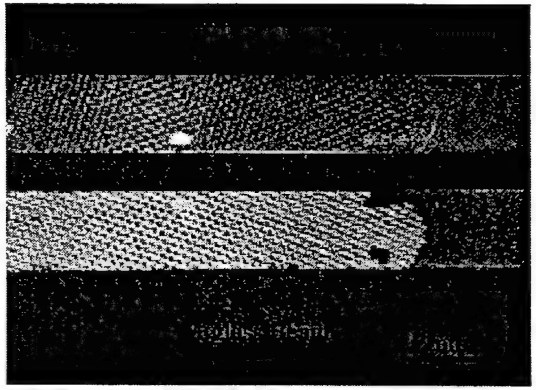

a- 1 day

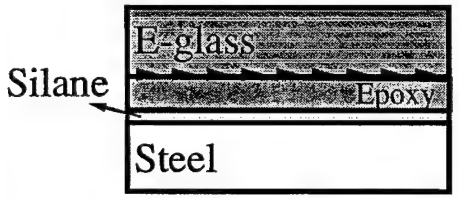

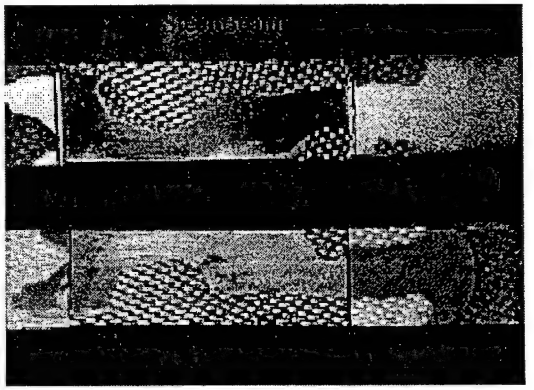

b- 5 days

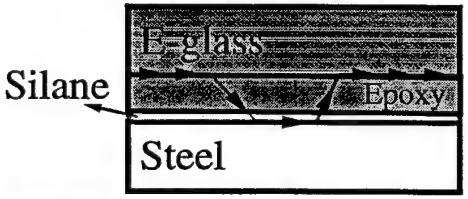

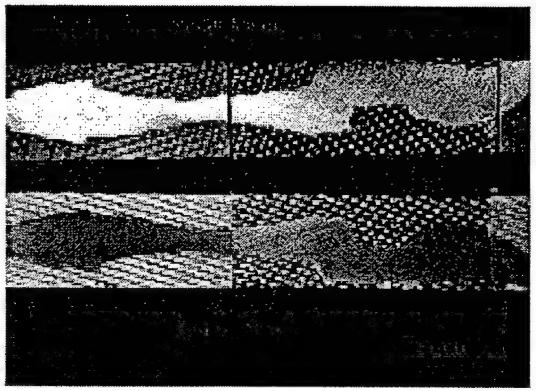

c- 10 days

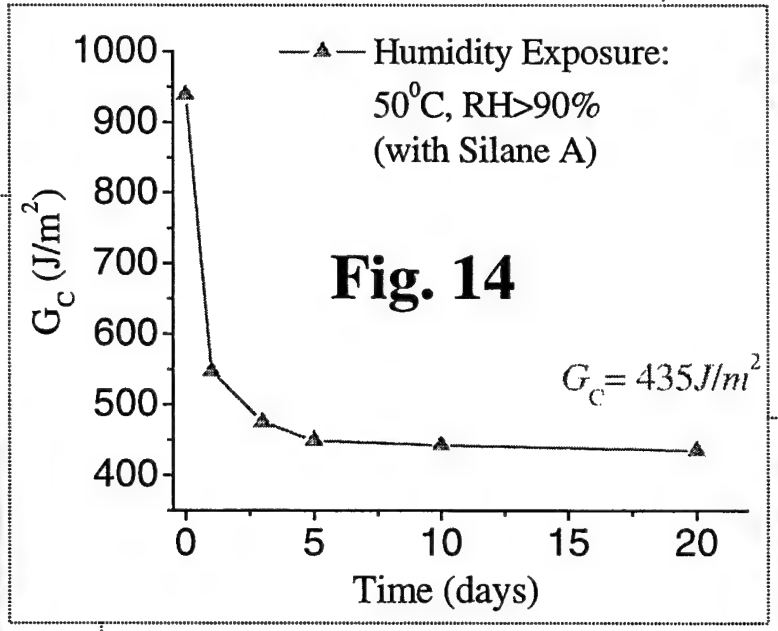

Fig. 14

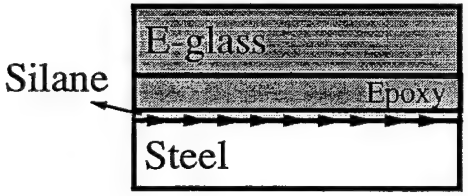

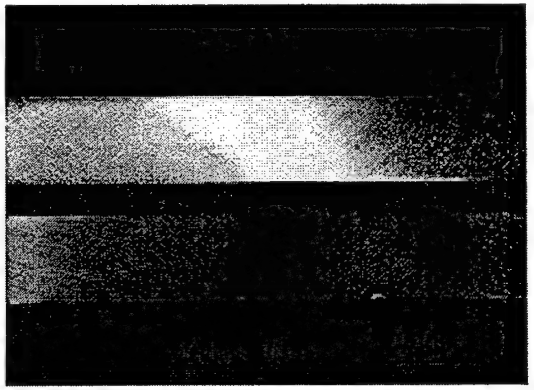

d- 20 days

Steel/Silane(A)/Epoxy/E-glass (After 1 day Humidity Exposure)

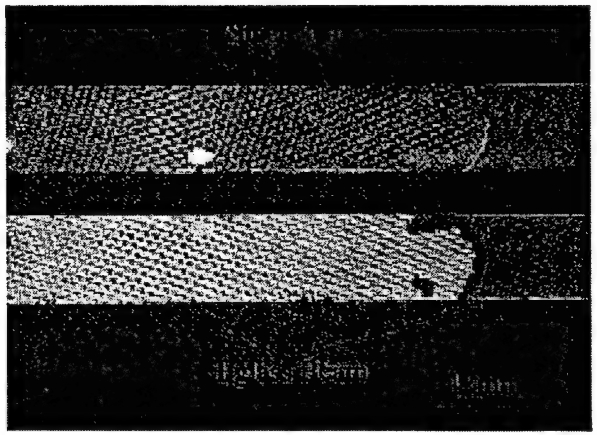

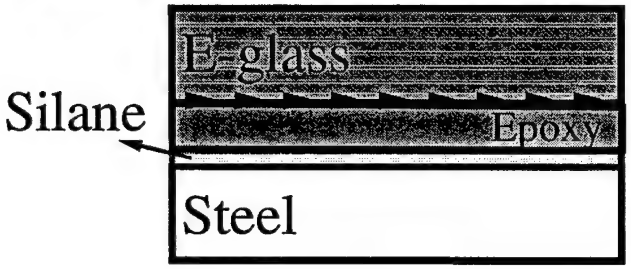

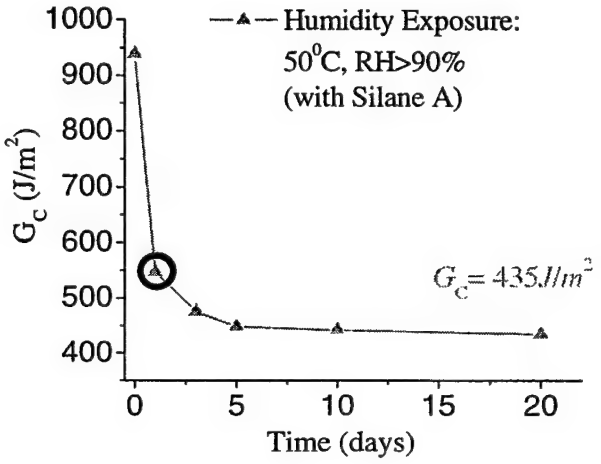

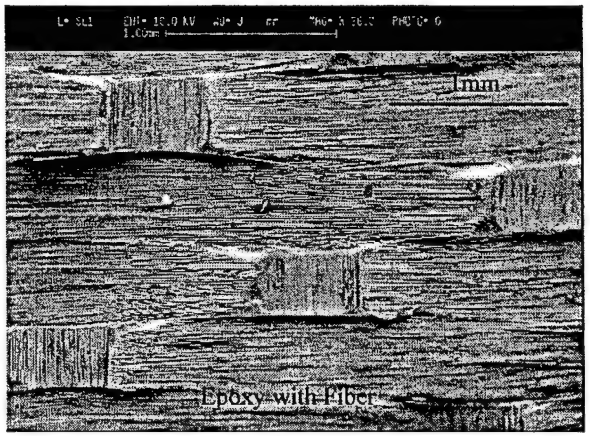

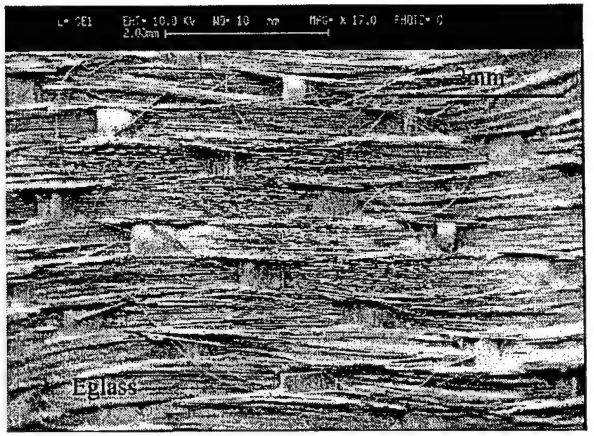

crack surfaces

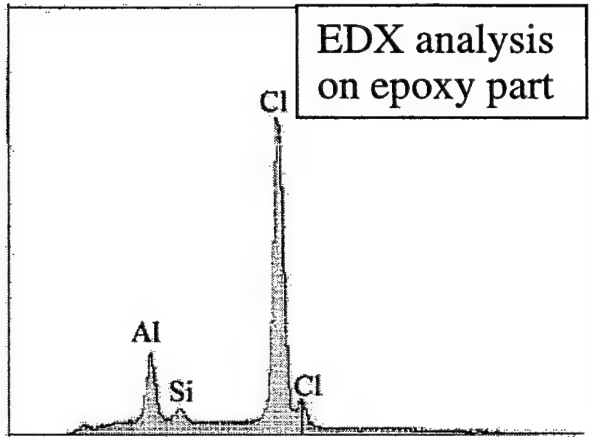

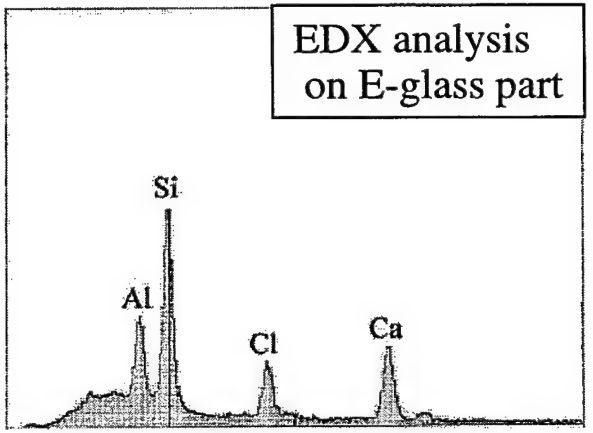

EDX analysis

Fig. 15

Steel/Silane(A)/Epoxy/E-glass (After 10 days Humidity Exposure)

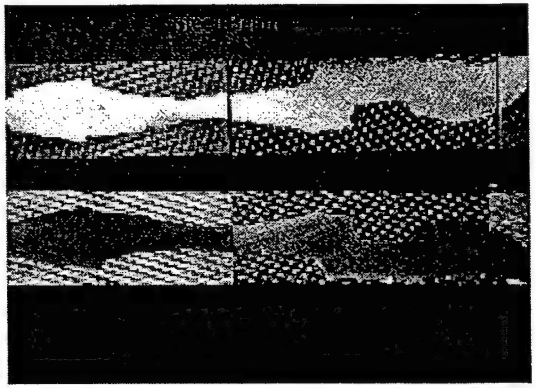

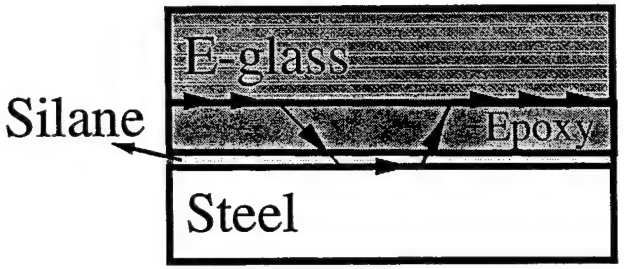

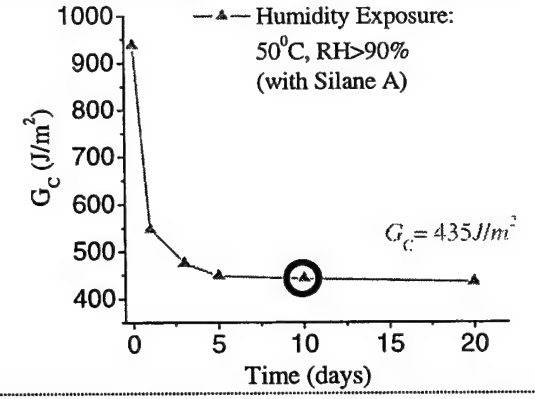

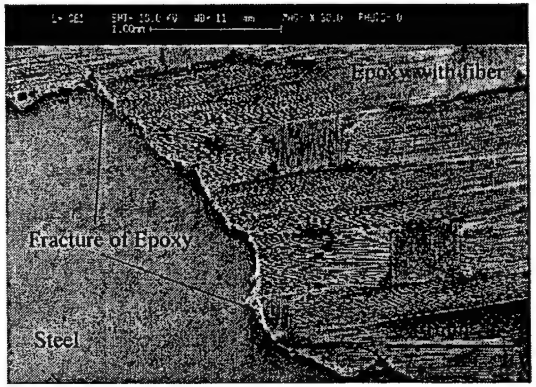

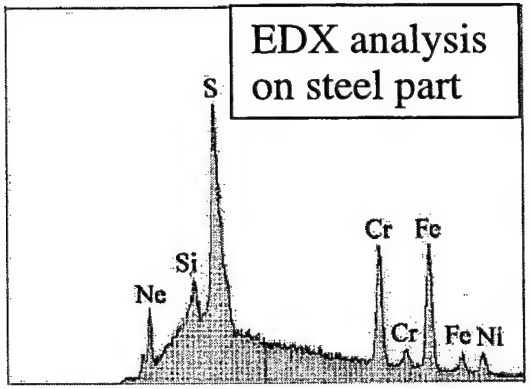

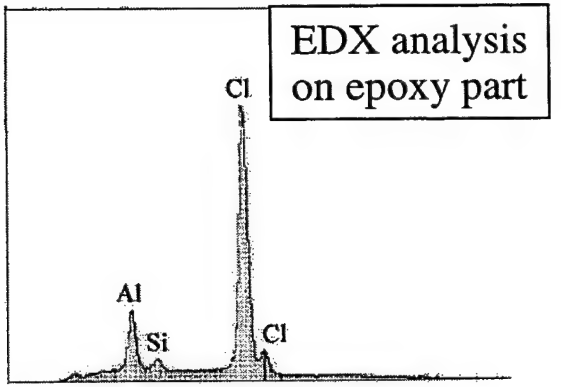

steel beam with some epoxy attached

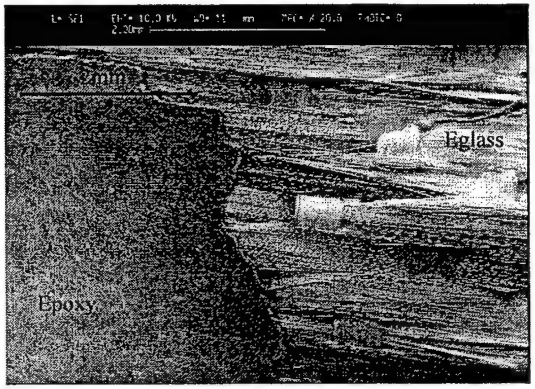

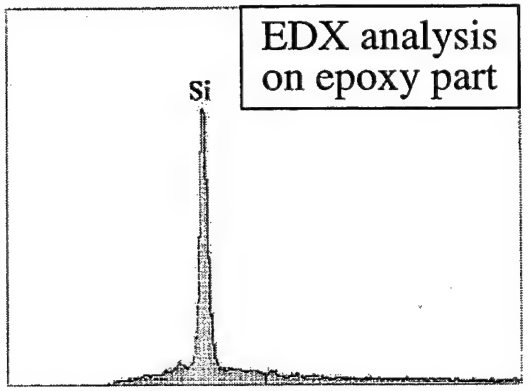

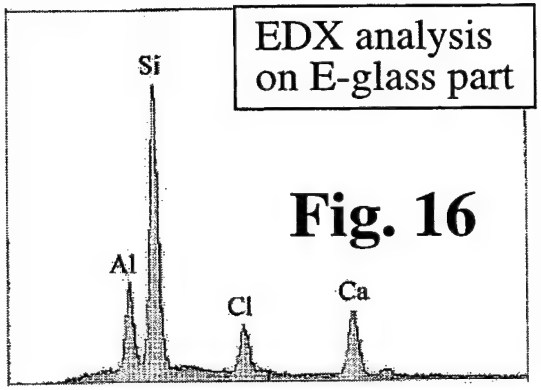

Fig. 16

E-glass beam with some epoxy attached

Steel/Silane(A)/Epoxy/E-glass (After 20 days Humidity Exposure)

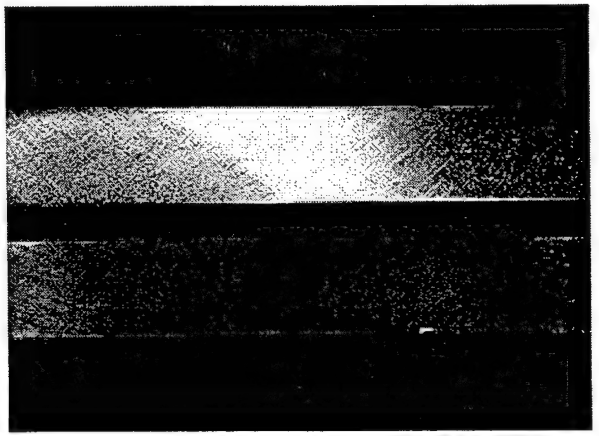

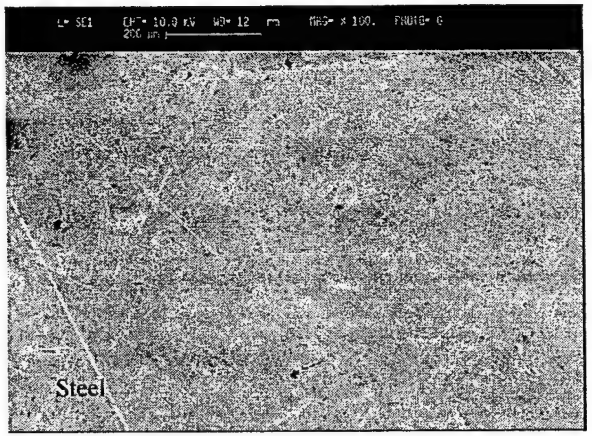

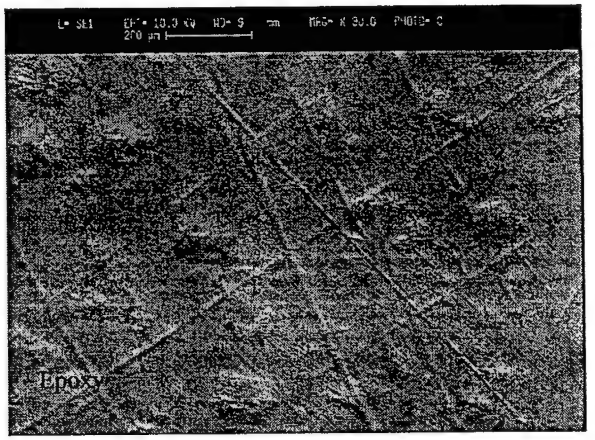

crack surfaces

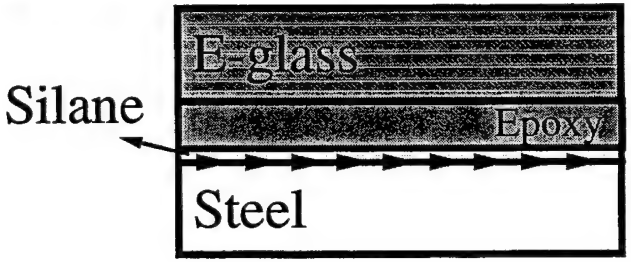

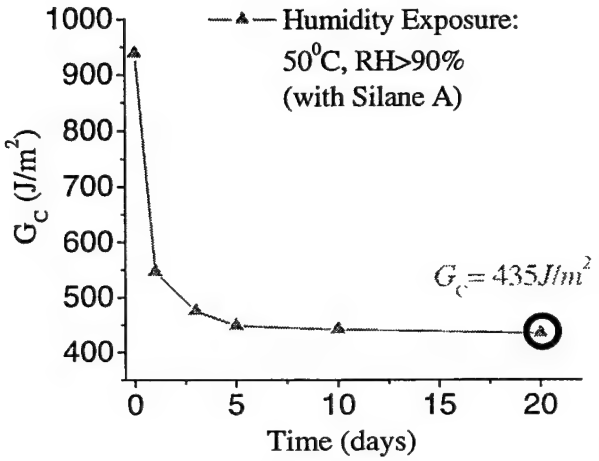

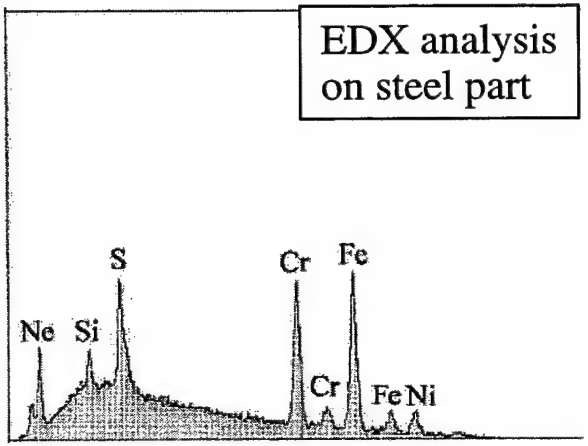

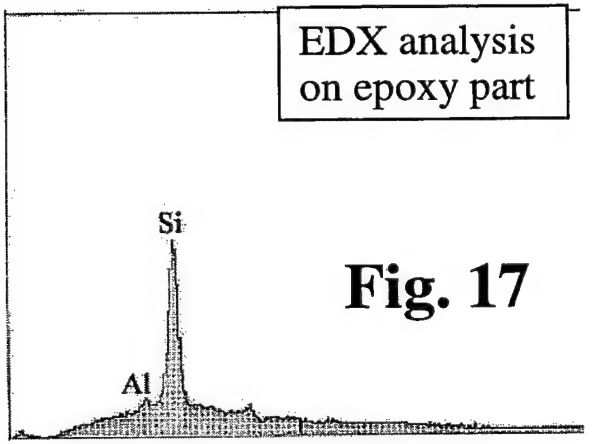

Fig. 17

EDX analysis

Effect of Humidity on Fracture Energies of Joints Steel/Silane(B)/Epoxy/E-glass

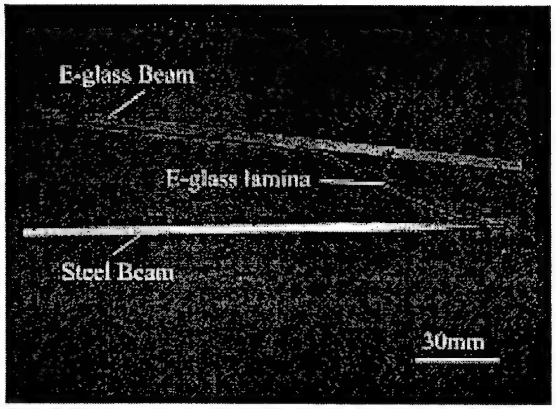

a- 1 day

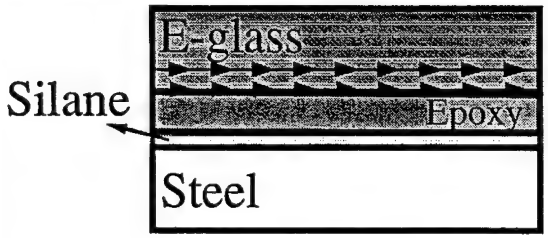

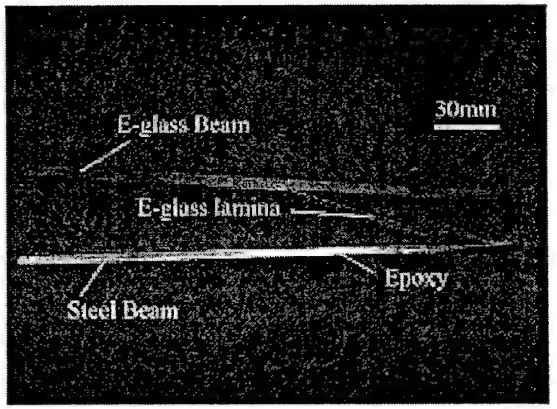

b- 5 days

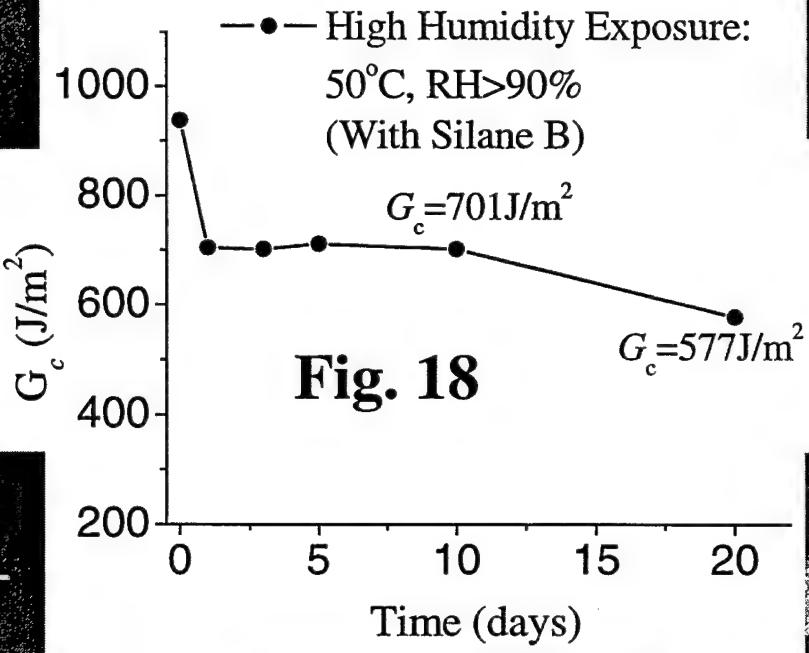

Fig. 18

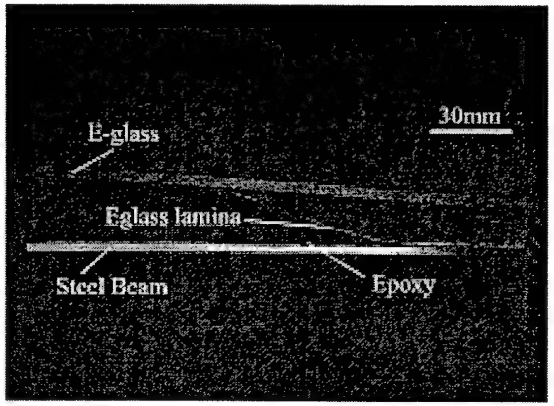

c- 10 days

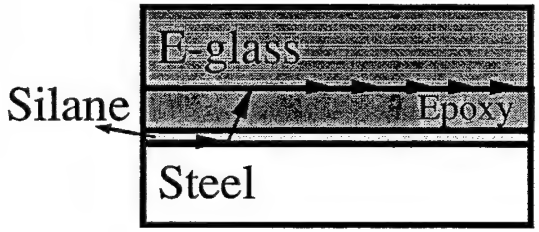

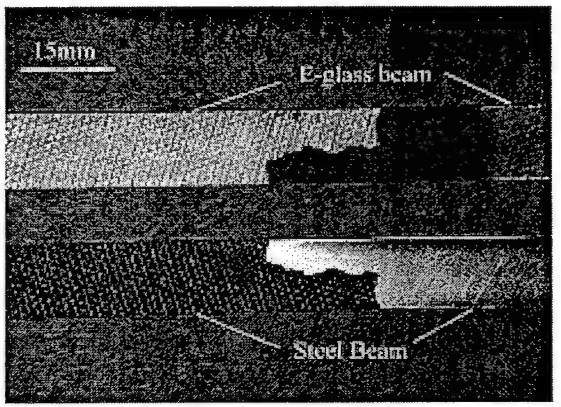

d- 20 days

Effect of Seawater on Fracture Energies of Steel/E-glass Joints

Table 1. Composition of Seawater

Element	ppm
Chlorine, Cl	19,500
Sodium, Na	10,770

Note: ppm= parts per million = mg/litre = 0.001g/kg

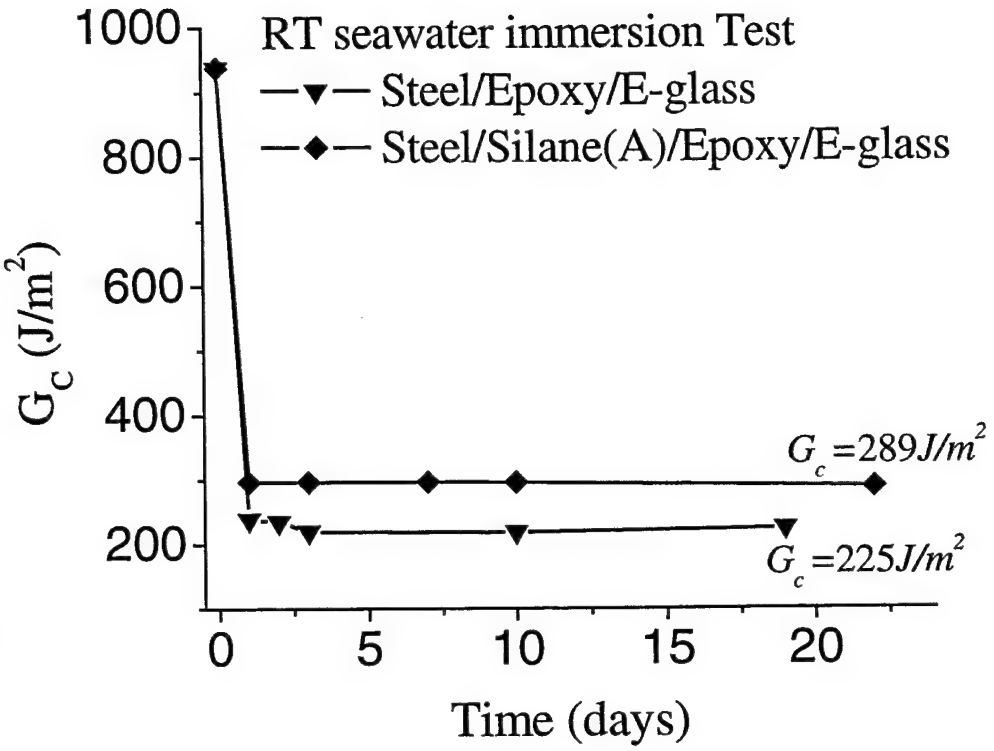

Fig. 19

Effect of Seawater on Fracture Energies of Joints Steel/Epoxy/E-glass

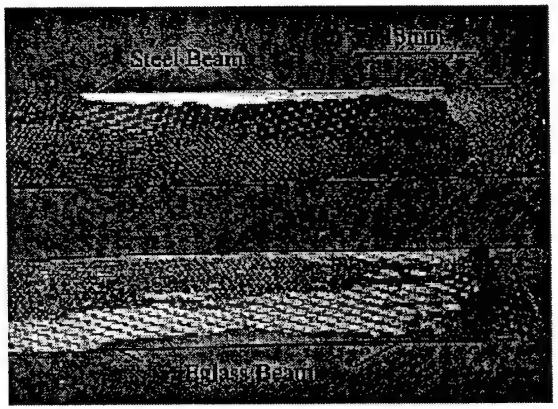

a- 1 day

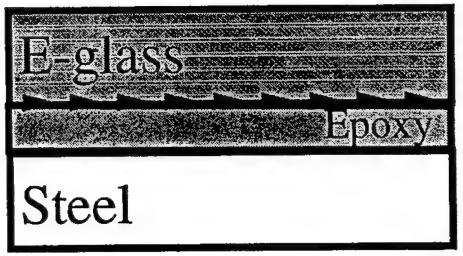

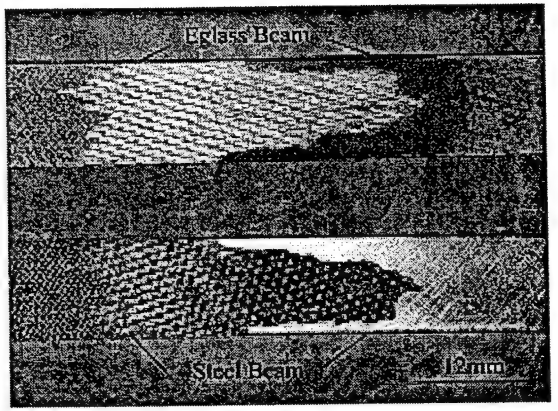

b- 3 days

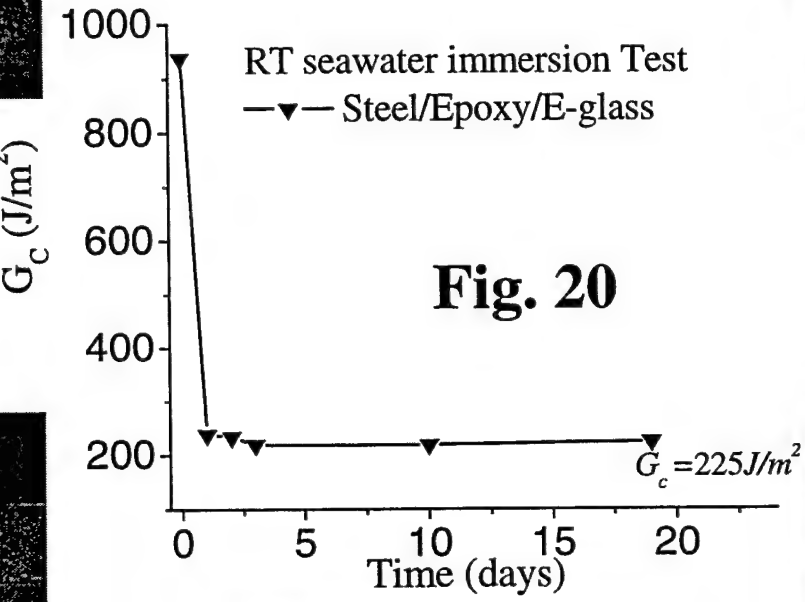

Fig. 20

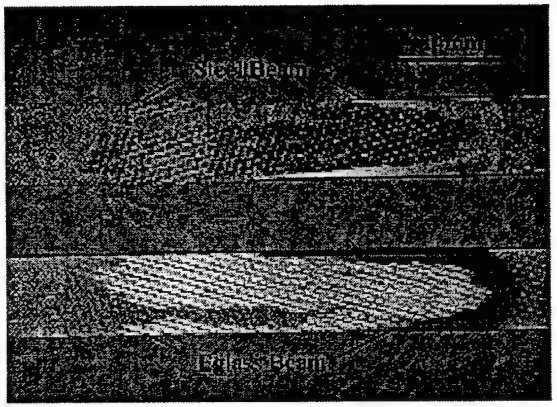

c- 10 days

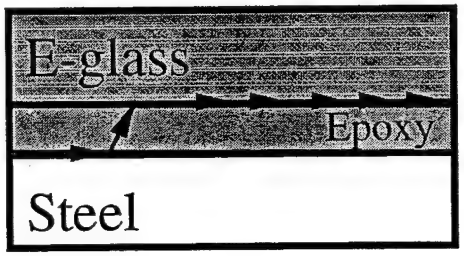

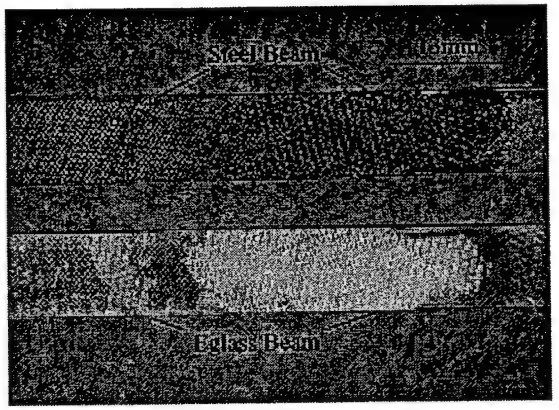

d- 19 days

Effect of Seawater on Fracture Energies of Joints Steel/Silane(A)/Epoxy/E-glass

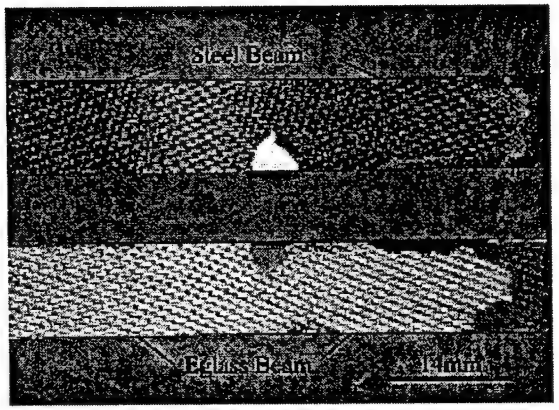

a- 1 day

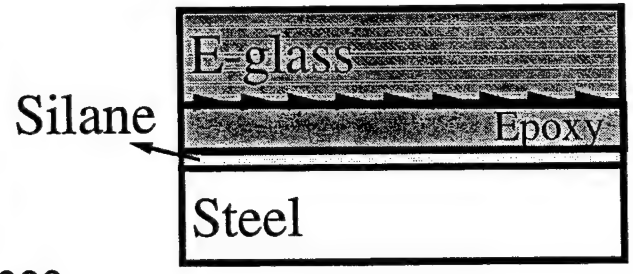

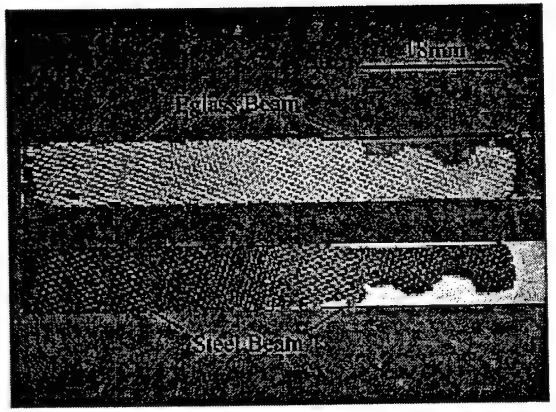

b- 3 days

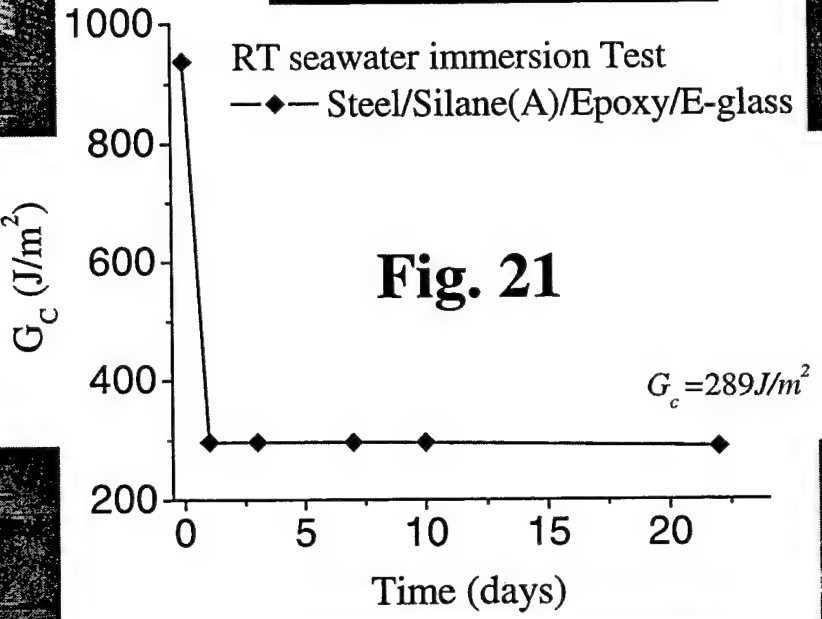

Fig. 21

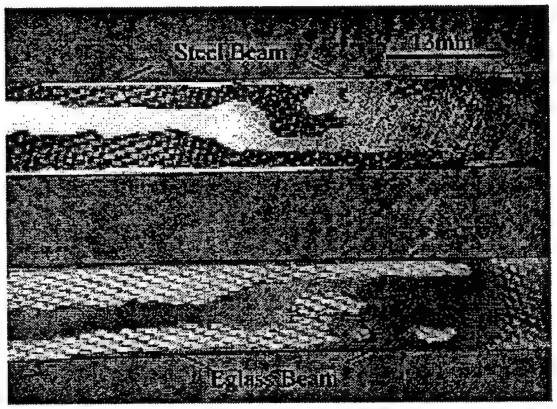

c- 7 days

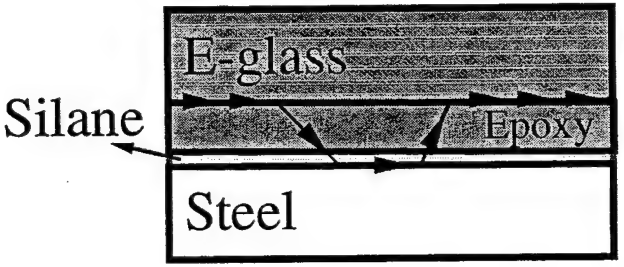

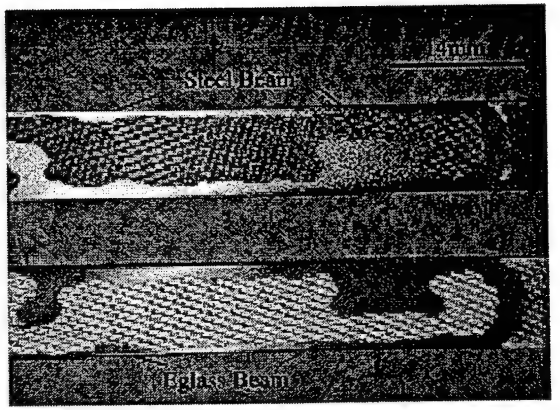

d- 22 days

Steel/Epoxy/E-glass (after 1 day seawater immersion)

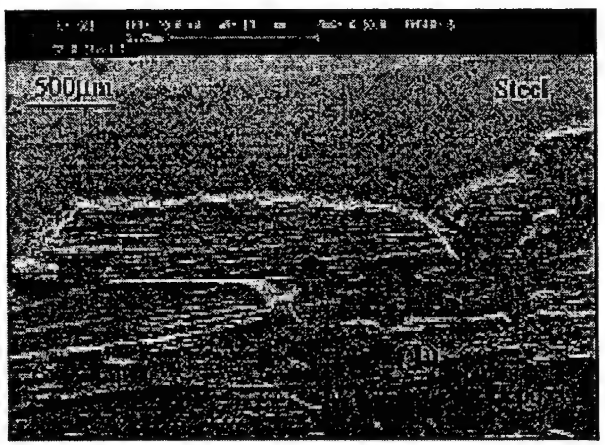

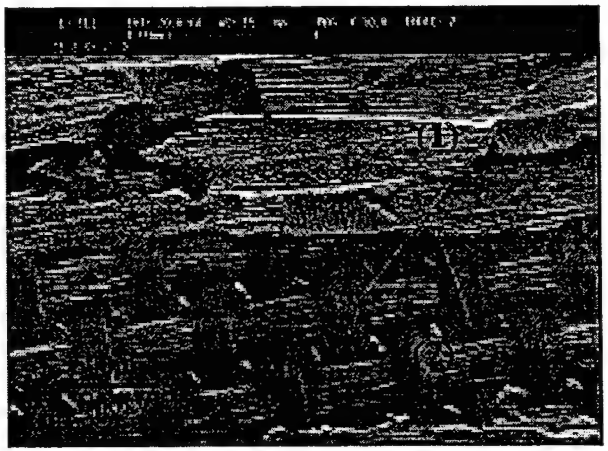

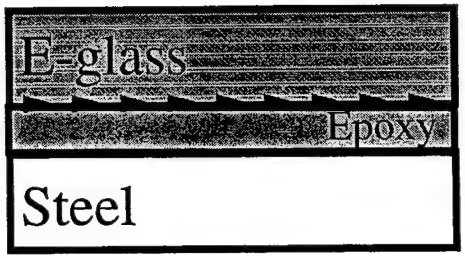

a. SEM: fracture surface of steel beam with some epoxy attached

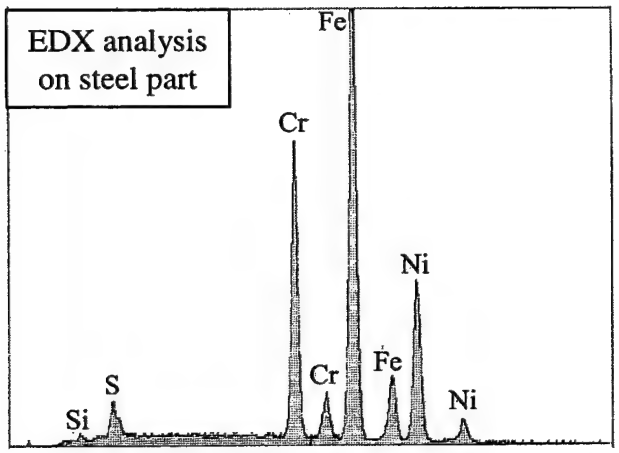

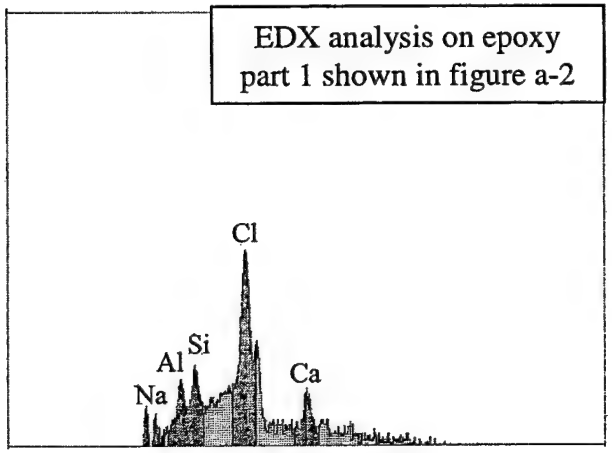

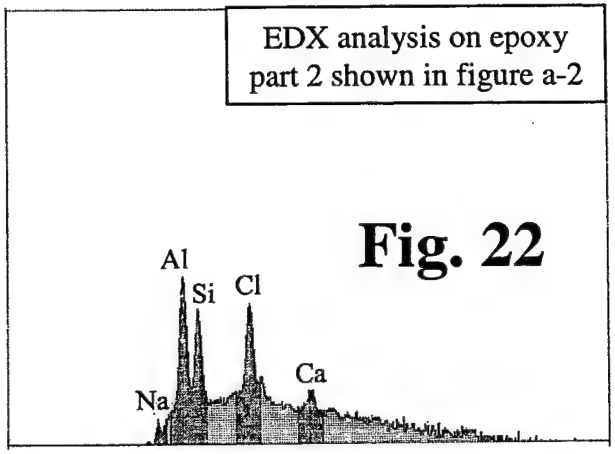

Fig. 22

b. EDX analysis on the part shown in figure a

Steel/Epoxy/E-glass (after 1 day seawater immersion)

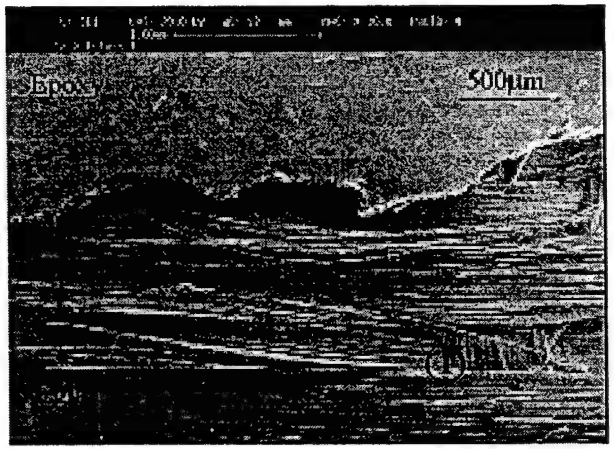

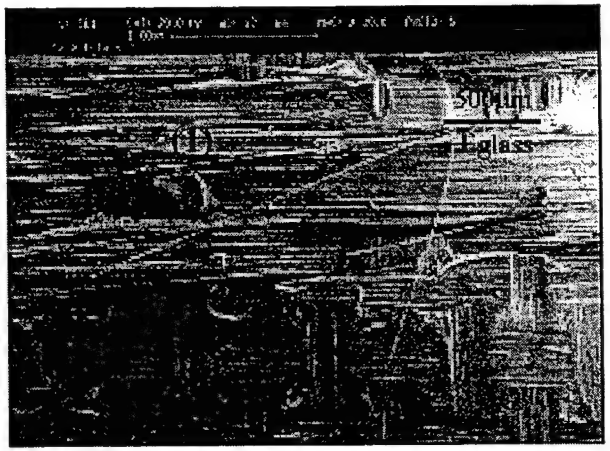

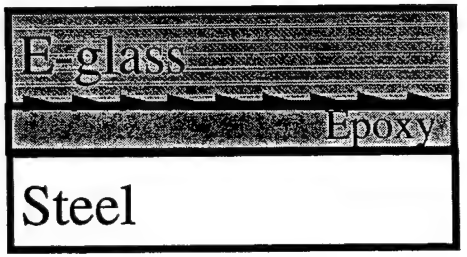

c. SEM: fracture surface of E-glass beam with some epoxy attached

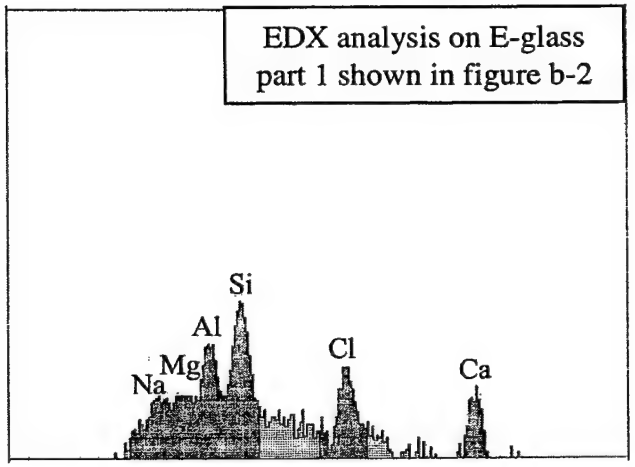

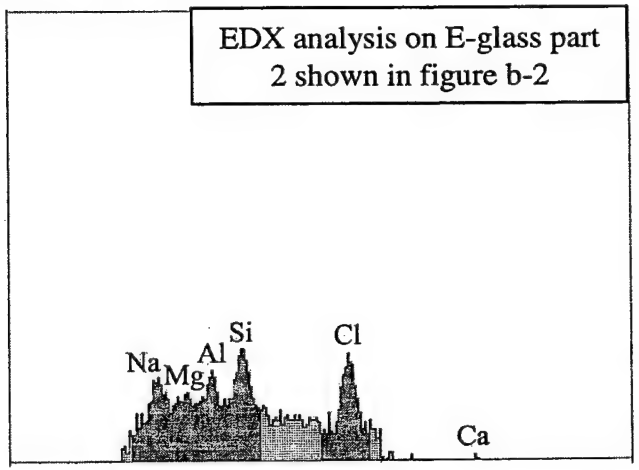

Fig. 23

d. EDX analysis on the part show in figure c
Note: There is no signal on the epoxy part

Steel/Silane(A)/Epoxy/E-glass (after 1 day seawater immersion)

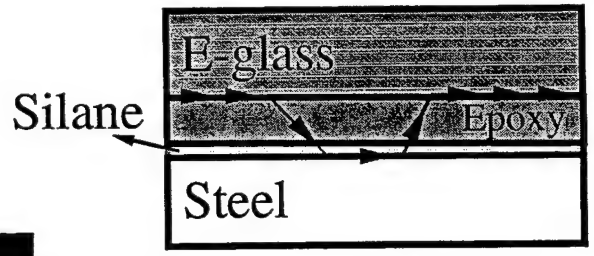

Fig. 24

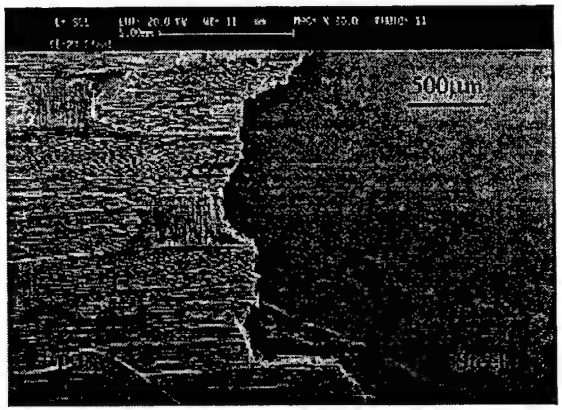

a. fracture surface of steel beam with some epoxy attached

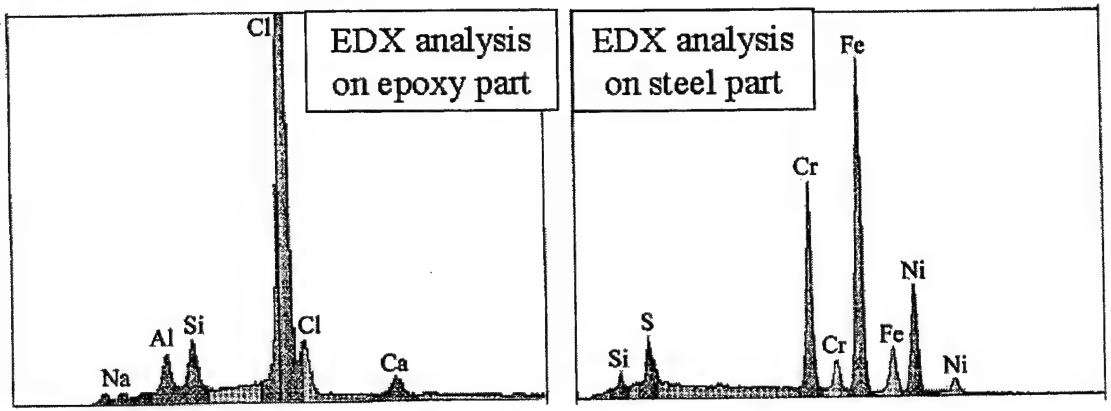

b. EDX analysis on the part shown in figure a

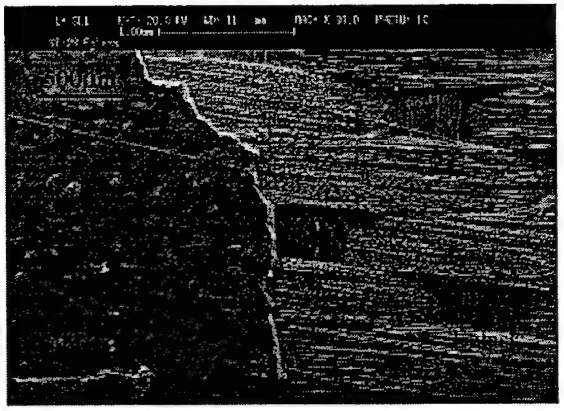

c. fracture surface of E-glass beam with some epoxy attached

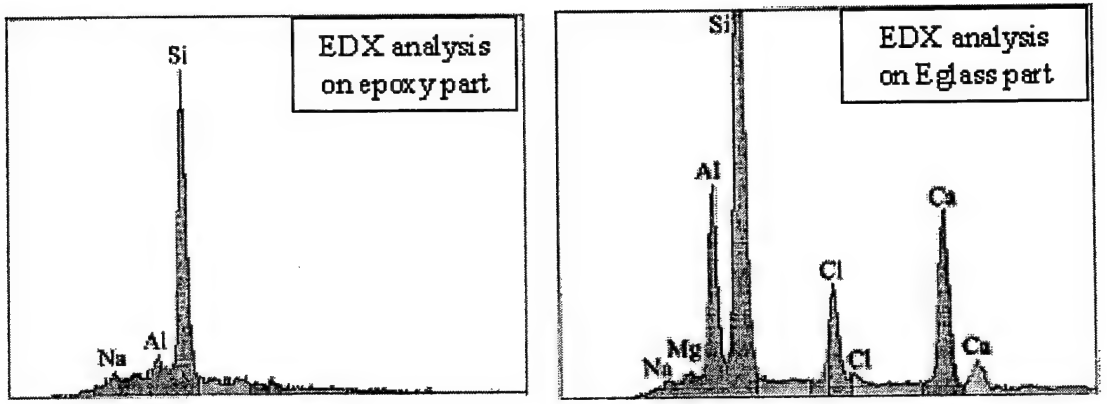

d. EDX analysis on the part shown in figure c

Summary of Effects of Moisture and Seawater on the Fracture Energies of Steel/E-glass Joints

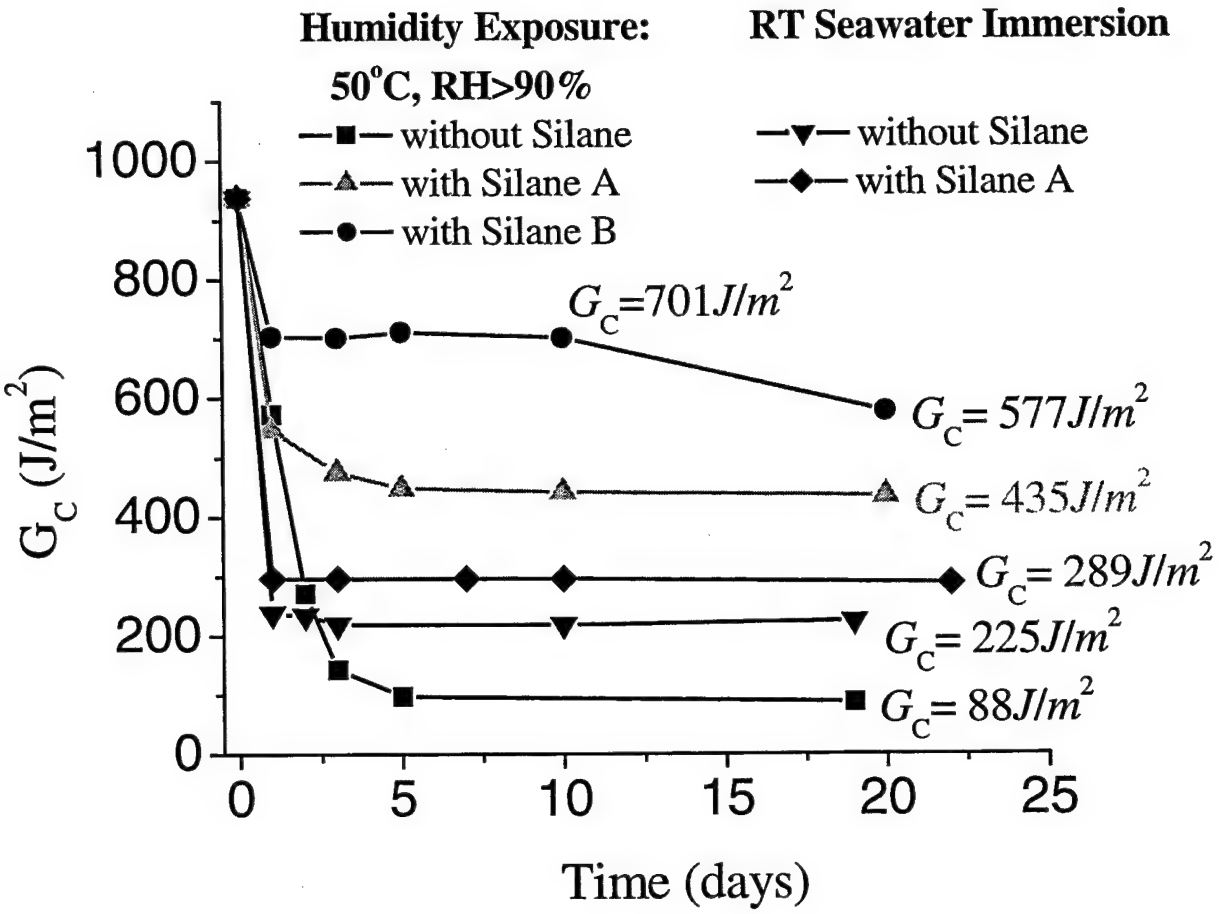

Fig. 25

Effect of Cryogenic Temperature on Fracture Energies of Steel/E-glass Joints

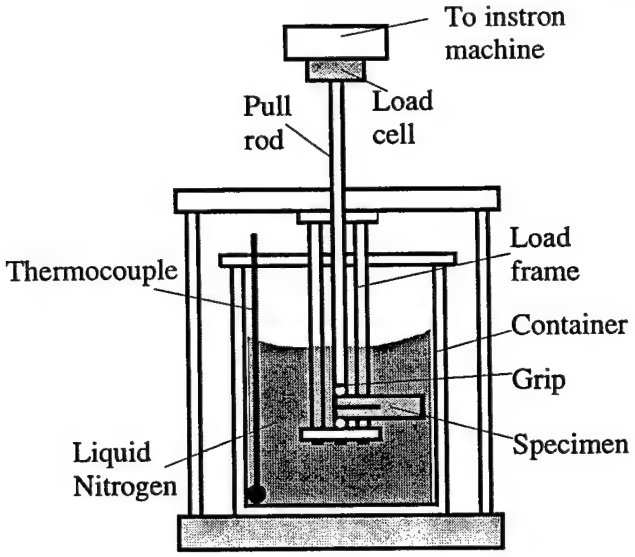

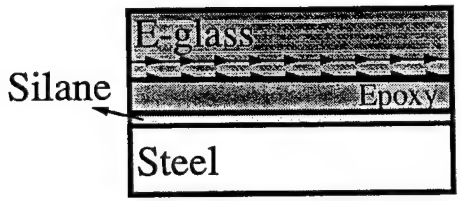

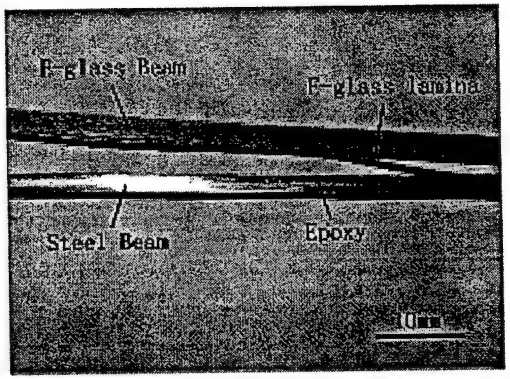

a. Observed failure in steel/epoxy/E-glass joint at liquid nitrogen temperature of 77K

Fig. 26

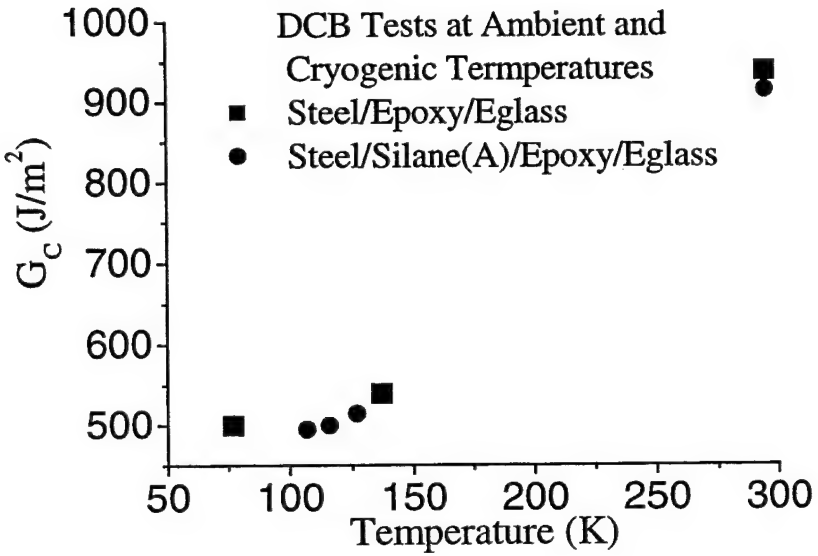

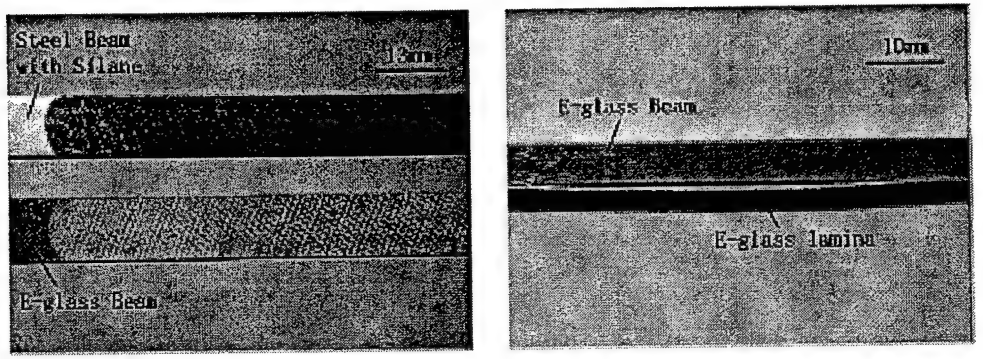

b. Observed failure in steel/silane(A)/epoxy/E-glass joint at liquid nitrogen temperature of 77K

Steel/Epoxy/E-glass at 77K

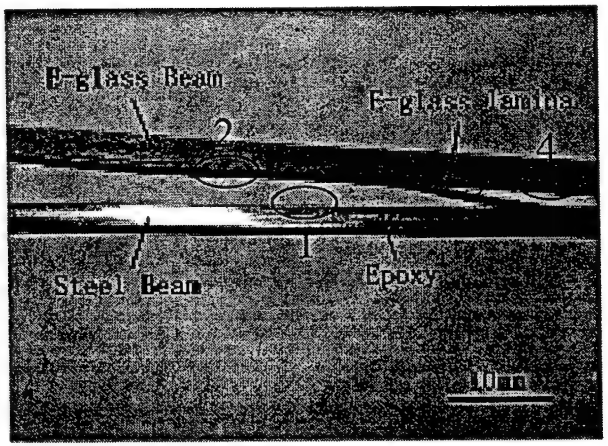

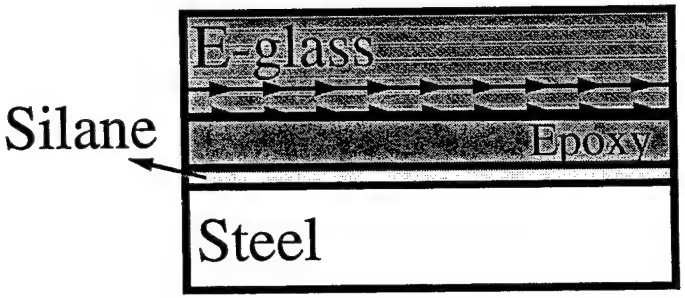

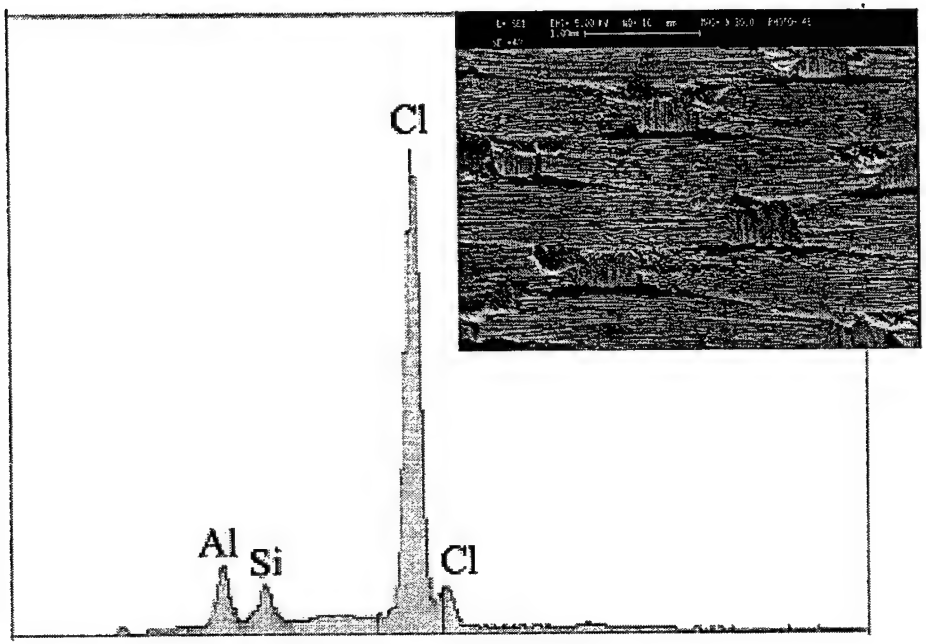

SEM and EDX at Region 1 – Epoxy on steel Beam

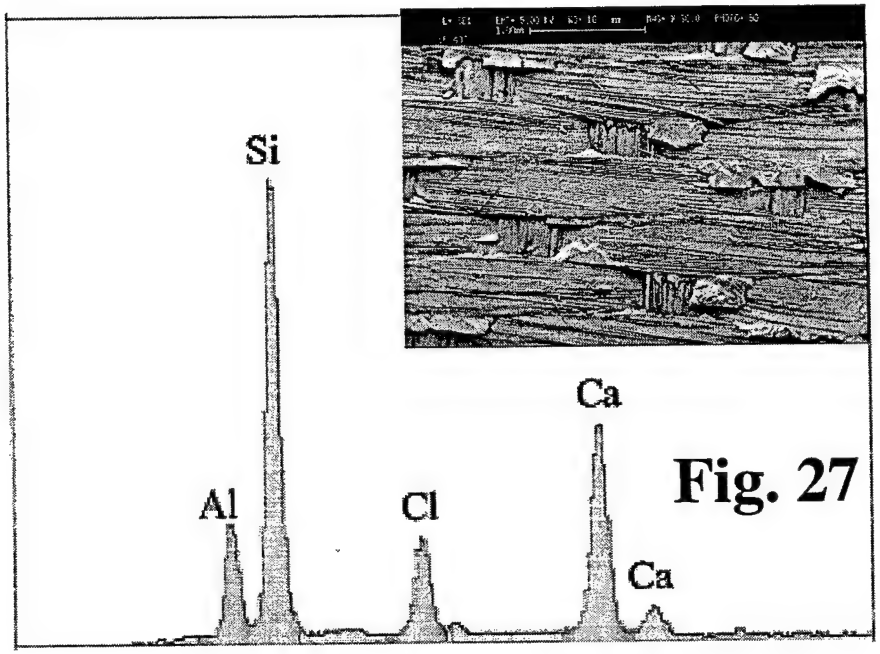

SEM and EDX at Region 2 – Composite

Fig. 27

Steel/Epoxy/E-glass at 77K

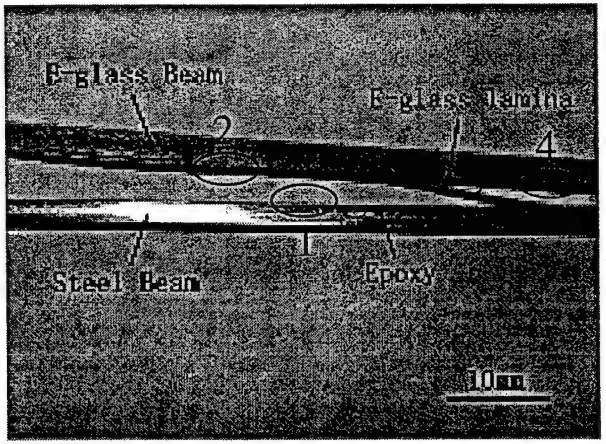

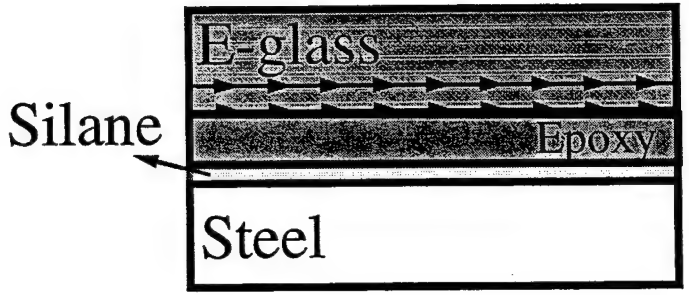

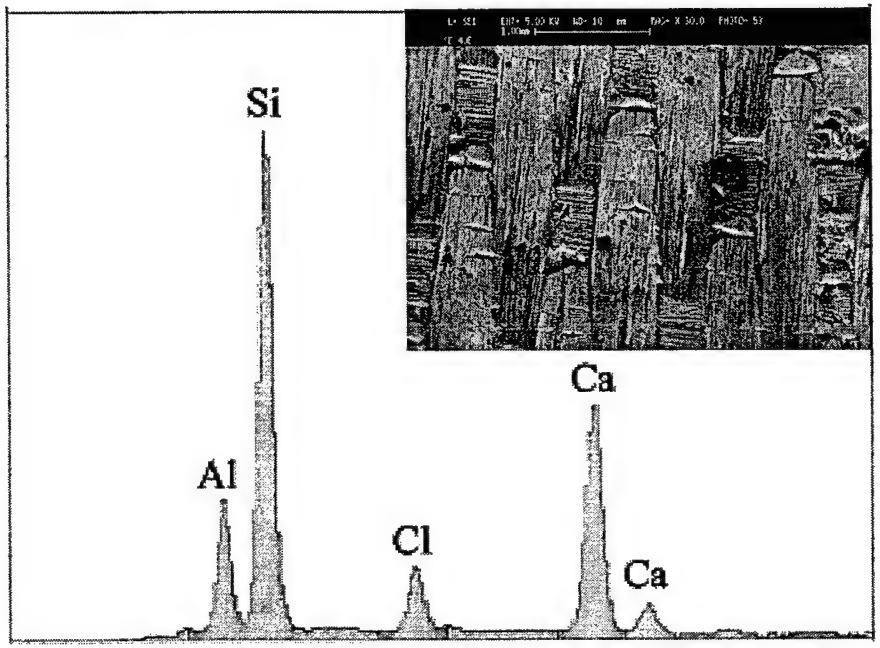

SEM and EDX at Region 3 – Composite ply

Fig. 28

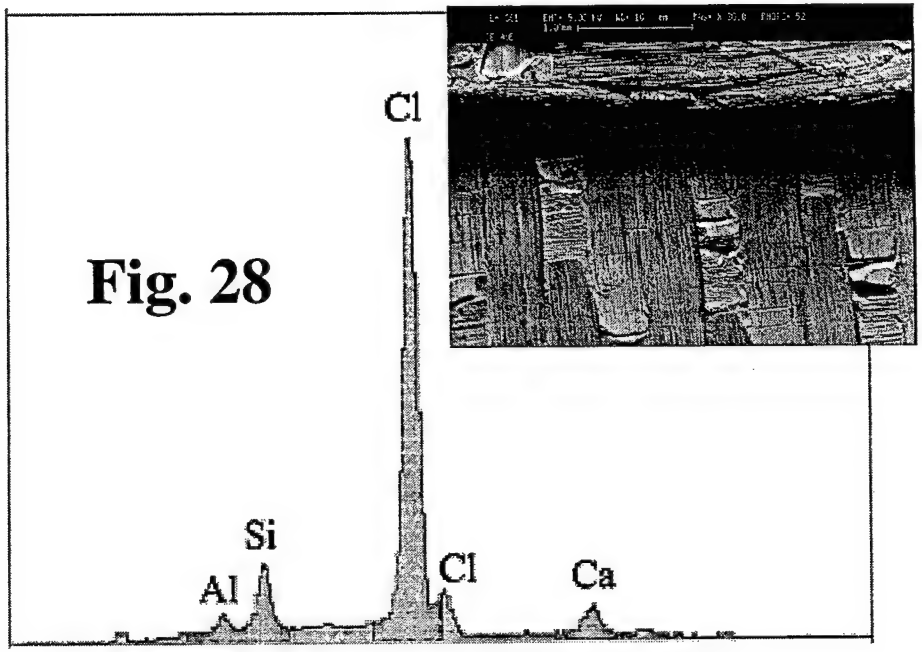

SEM and EDX at Region 4 – Composite

Steel/Silane(A)/Epoxy/E-glass at 77K

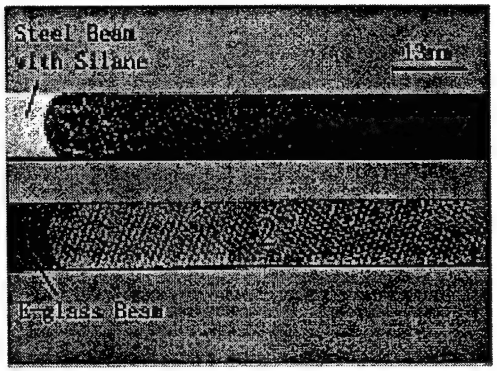

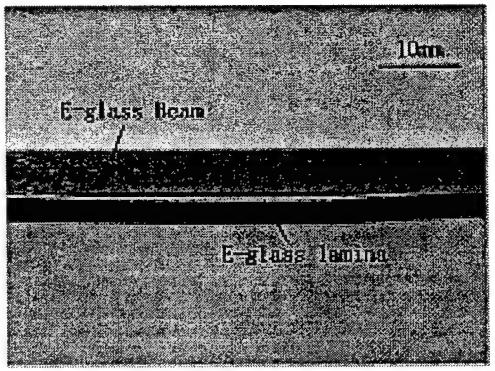

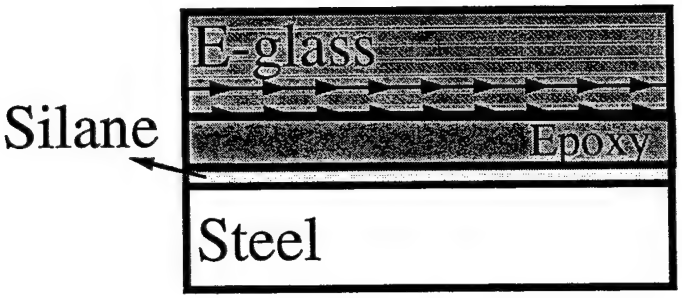

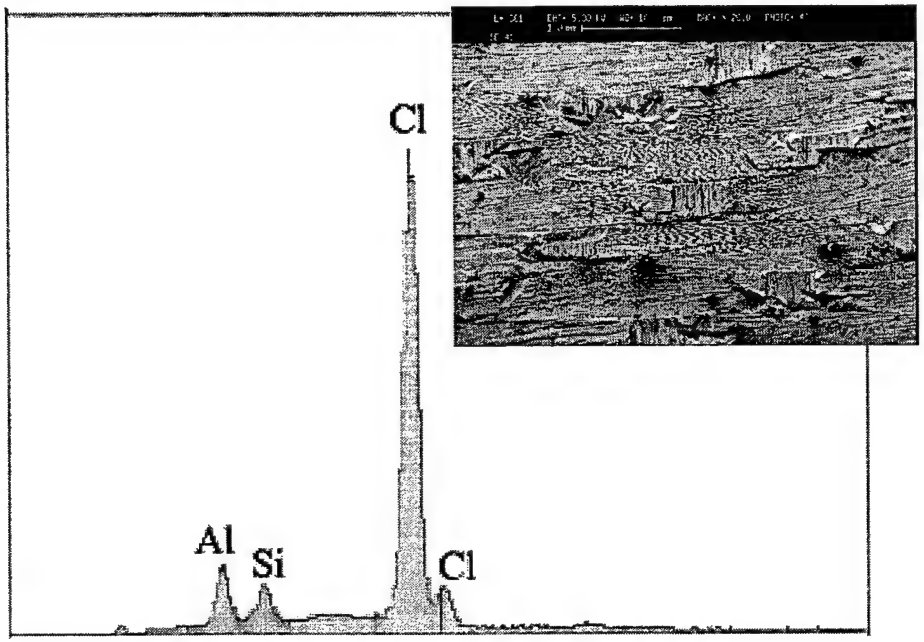

SEM and EDX at Region 1 – Epoxy on steel Beam

Fig. 29

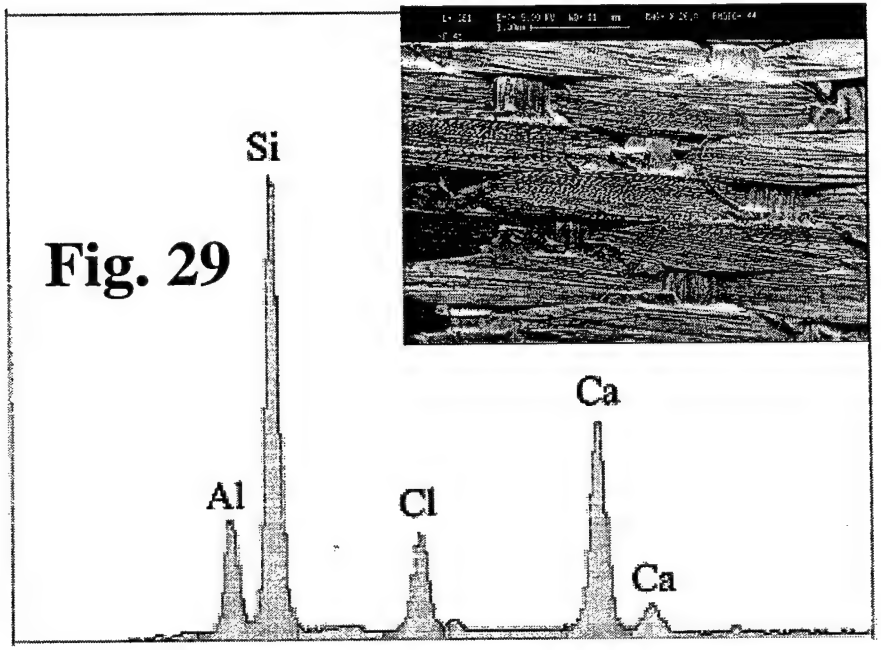

SEM and EDX at Region 2 – Composite

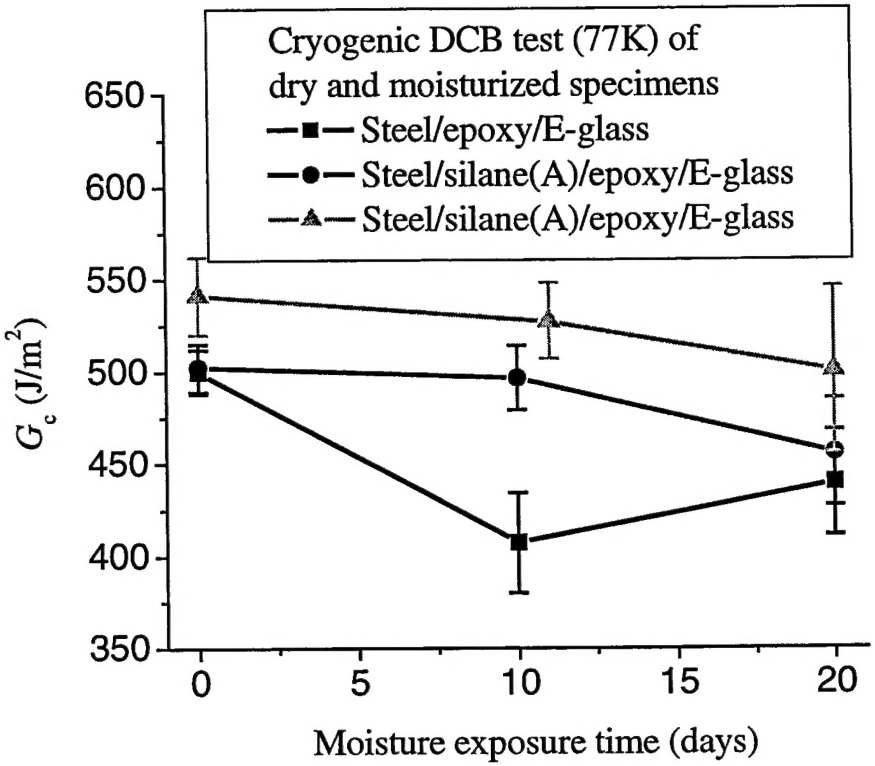
Cryogenic DCB test (77K) of
dry and moisturized specimens
Steel/epoxy/E-glass
Steel/silane(A)/epoxy/E-glass
Steel/silane(A)/epoxy/E-glass
650
600
550
500
450
400
350
G_c (J/m^2)
0
5
10
15
20
Moisture exposure time (days)

Fig. 30

Dynamic Measurement of σ_0 of Steel/E-glass joints by using Laser-generated Stress Pulses

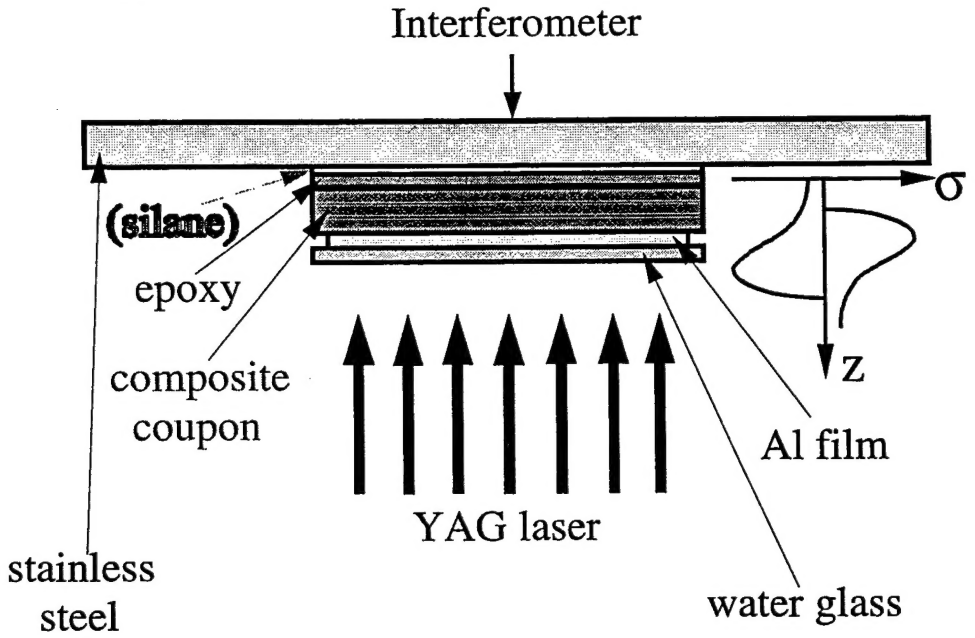

Table 2. Tensile strengths σ_0 of various interfaces

Interface	Incident fluence (mJ/mm^2)	σ_0(MPa)
Composite/epoxy	39.8 ± 0.2	198 ± 13
Steel/epoxy	41.4 ± 0.5	171 ± 16
Steel-silane(A)/epoxy	53.6 ± 0.2	224 ± 13
Steel-silane(B)/epoxy	37.2 ± 0.2	250 ± 13

Fig. 31

Failure Mechanisms

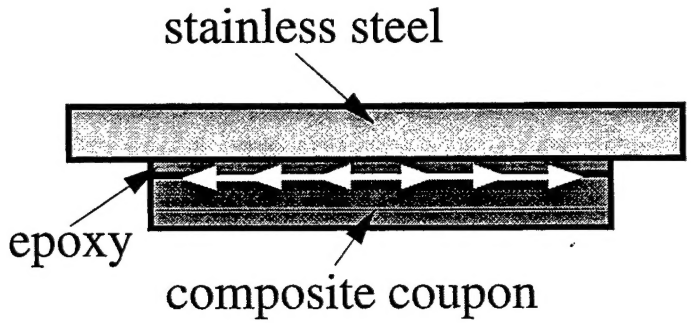

(a) Laser fluence: 38.2 ± 0.2 mJ/mm^2

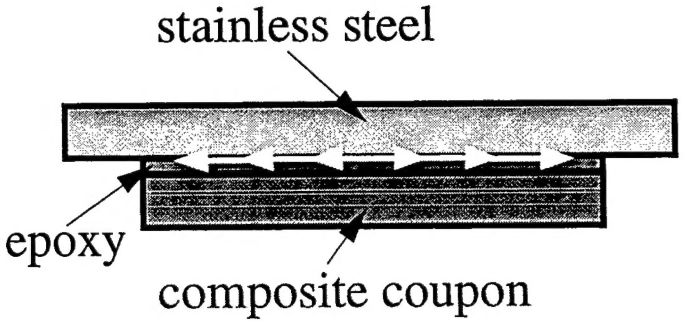

(b) Laser fluence: 41.4 ± 0.5 mJ/mm^2

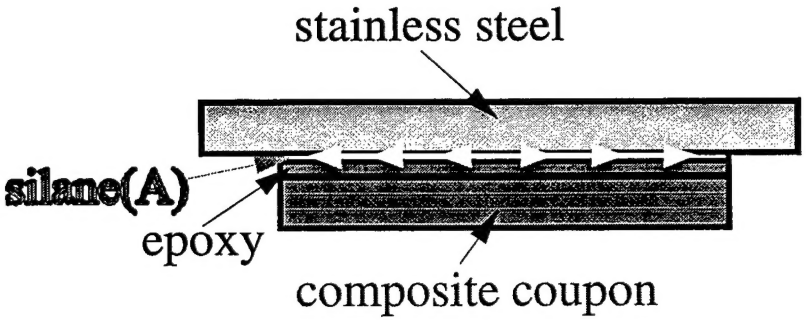

(c) Laser fluence: 53.6 ± 0.2 mJ/mm^2

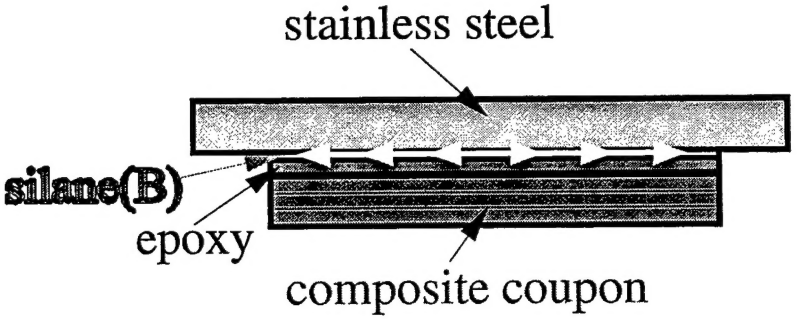

(d) Laser fluence: 57.2 ± 0.2 mJ/mm^2

Fig. 32

Spallation of steel/E-glass sample under ambient conditions

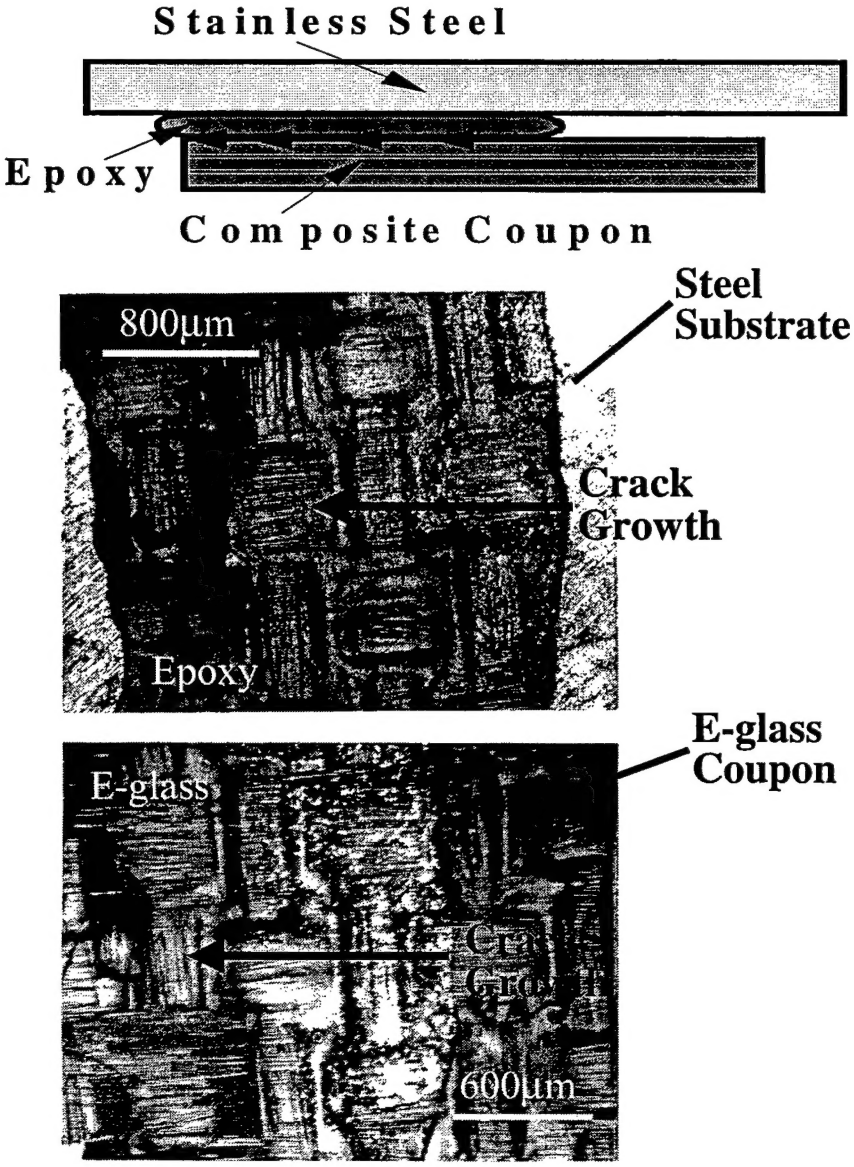

Spallation of steel/E-glass sample after two-day-humidity-exposure

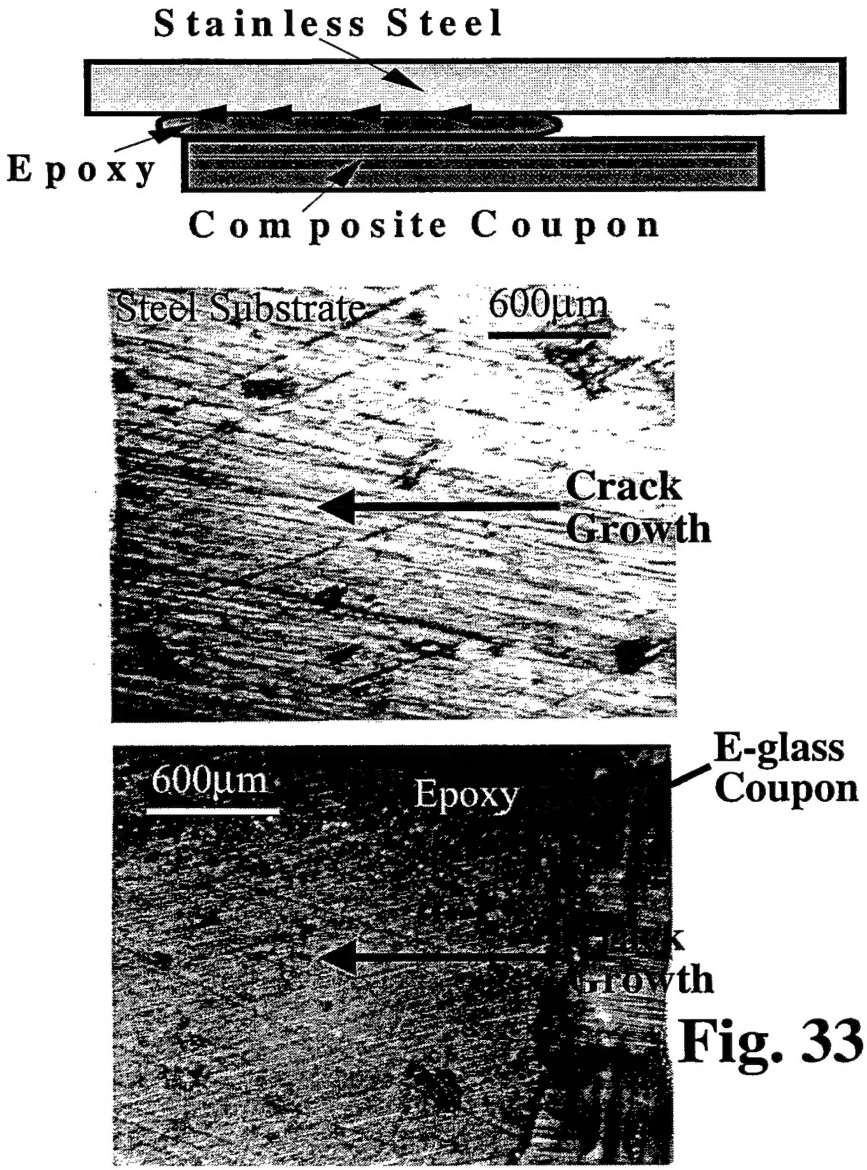

Fig. 33